https://doi.org/10.1070/RCR4991

Titanium dioxide nanotubes: synthesis, structure, properties and applications

Andrey A. Rempel,[a, c] Albina A. Valeeva,[b, c] Alexander S. Vokhmintsev,[c] Ilya A. Weinstein [a, c]

[a] *Institute of Metallurgy, Ural Branch of the Russian Academy of Sciences, ul. Amundsena 101, 620016 Ekaterinburg, Russian Federation*
[b] *Institute of Solid State Chemistry, Ural Branch of the Russian Academy of Sciences, ul. Pervomaiskaya 91, 620108 Ekaterinburg, Russian Federation*
[c] *Ural Federal University, ul. Mira 19, 620002 Ekaterinburg, Russian Federation*

Methods of synthesis of nanotubular structures based on titania of various phase and chemical compositions are described. A systematic account is given of known data about the influence of synthesis and subsequent treatment conditions on the amorphous and crystal structures, specific surface area, morphology and optical, luminescence and electro-physical properties of titania-based nanotubular oxide materials. The photocatalytic properties in the oxidation reactions of organic compounds and the performance characteristics of the memristive behaviour of TiO_2-based nanotubular structures are considered in details. Their applications are discussed.
The bibliography includes 238 references.

Contents

1. Introduction 1397
2. Methods of synthesis 1398
   2.1. Template, sol – gel and hydro(solvo)thermal methods 1398
   2.2. Electrochemical synthesis, anodization 1399
3. Structure 1401
   3.1. Atomic structure 1401
   3.2. Electronic structure, nonstoichiometry 1401
   3.3. Modification of structure and phase composition 1402
   3.4. Modification of functional properties 1403
4. Applications 1404
   4.1. Heterogeneous photocatalysis 1404
   4.2. Nanoelectronics, memristors 1405
   4.3. Power engineering, betavoltaics 1406
   4.4. Supercapacitors 1407
5. Note added in proof 1409
6. Conclusion 1409
7. List of acronyms and designations 1410

1. Introduction

Titanium dioxide (titania, TiO_2) with extensive surface area is an economically available functional material, and, regarding the environment conservation, it is non-toxic and safe during the production and use.[1 – 11] Titanium dioxide has been long and widely used as a solid-state base for the development of high-performance photocatalytic cells, solar cells, sunscreening agents, paints, sensing and photochromic devices and biomedical implant coatings and for solving many other high-technology problems.[12 – 26] Titanium dioxide possesses a number of specific characteristics, which make it unique among transition metal oxides, such as high chemical inertness, corrosion resistance, stability to external stimuli, good biocompatibility and controlled activity in the near-UV and visible spectral regions of electromagnetic radiation.[12] The ability of efficient photogeneration of electron – hole pairs under the action of natural and laboratory optical radiation extends the scope of applicability of TiO_2 to water photolysis, hydrogen production and other potentially green energy-saving processes.[21 – 23] In 1972, Fujishima and Honda [21] reported for the first time the electrochemical photolysis of water under the action of UV radiation using TiO_2-based electrodes. Currently, titanium dioxide can be regarded as one of the most well-known, but still being most actively studied compounds in materials science.

In the last decade, titanium dioxide nanotubes (TiO_2 NTs) have attracted increasing attention of researchers due to the prospects for their use as high-performance photocatalysts to synthesize organic compounds according to green chemistry principles.[27 – 33] It is expected that non-stoichiometric titanium dioxide will be most useful for modern photocatalysis, because this material absorbs visible light. Stoichiometric TiO_2 does not absorb visible light; therefore, exposure to the harmful and expensive UV radiation is required for its functioning. An efficient way for increasing the titanium dioxide non-stoichiometry is to generate structural defects, in particular, oxygen vacancies, which would change the optical and electronic properties of the material. The point defects present in the crystal lattice give rise to additional levels in the energy gap of TiO_2, which, in turn, causes a decrease in the efficient band gap and a shift of the photosensitivity to the visible range.[34 – 39]

These changes result in a considerable increase in the photocatalytic activity towards oxidation of organic molecules, hydrogen evolution from aqueous solutions and synthesis of organic compounds. This is favourable for

Received 7 August 2020
© 2021 Uspekhi Khimii, ZIOC RAS, Russian Academy of Sciences and IOP Publishing Limited

increasing the efficiency of air and water purification from organic pollutants, production of hydrogen and green drug production processes.

The pioneering studies on the synthesis of multi-walled [40] and single-walled [41] carbon nanotubes revolutionized the preparation and study of the unique properties of materials with a nanotubular morphology. Owing to high expectations from the possible scientific breakthroughs on the way towards combining the unique shape and functionality, where properties directly depend on the geometry (diameter, wall thickness, aspect ratio, *etc.*), the efforts of top-level scientists were focused on nanotechnologies, including chemical, physical and biomedical areas. In particular, the intensive search and testing of procedures for the synthesis of well-known oxides and sulfides in the nanotubular form were initiated.[42–44] It is noteworthy that the interest in natural and synthetic compounds with the indicated morphology was also expressed earlier in classical publications [45,46] on layered minerals and related structures (see also a review by Krivovichev [47]). Important information was gained on the common features of many compounds in the nanotubular form (*e.g.*, formation of nanotubes *via* spontaneous rolling-up of crystalline layers into nanoscrolls was found;[48] smooth variation of the component ratio across the nanotube diameter was demonstrated),[49] and their structures and physicochemical properties were studied.[47]

The first attempt to form TiO_2 NTs by anodization was described by Assefpour-Dezfuly *et al.*,[50] who used the alkaline treatment of titanium metal with hydrogen peroxide followed by electrochemical oxidation in a chromic acid-based electrolyte. In 1999, Zwilling *et al.*[51] reported the synthesis of self-organized arrays of titanium-supported nanotubes by anodization in chromic acid electrolytes containing fluoride ions. As a result, the number of publications addressing the physicochemical properties of titania nanotubes has sharply increased since the beginning of the 2000s. According to Scopus, an international scientific citation database, 1000–1250 such publications have appeared every year since 2011. The number of papers devoted to TiO_2 nanotubes synthesized by anodic oxidation accounts for ~30% of all publications dealing with anodic TiO_2 of any morphology. In recent years, detailed reviews [1,12,52–56] devoted to characteristic features of growth, modification methods, properties and versatile applications of TiO_2 nanotubes with brief description of approaches to their synthesis were published in top-ranked journals. The performed comparison of the known synthetic approaches demonstrated that the arrays of anodized TiO_2 nanotube have a number of undoubted benefits and an obvious potential for practical application; therefore, they attract considerable attention of researchers.

In comparison with other synthetic approaches such as hydro(solvo)thermal synthesis [57–59] and template synthesis involving the addition of structuring components (templates),[60,61] the direct electrooxidation proved to be more facile and high-performance method; using this method, it is possible both to gain and control the desired geometry at the nanoscale level by changing the size and shape and to improve the degree of ordering of nanotubes on the substrate by optimizing anodization conditions such as the applied voltage, current, time, temperature, pH and composition of the electrolyte.[52] Therefore, the resulting TiO_2 NT layers have a highly organized structure and an extensive specific surface area, show good mechanical strength, ensure unique electronic properties and high concentration and mobility of long-lived charge carriers, and exhibit various quantum confinement effects.[52,62] Furthermore, the electrochemical anodization is a relatively inexpensive process, which has prospects of a resource saving technology and is applicable to a broad range of transition metals.

2. Methods of synthesis

2.1. Template, sol–gel and hydro(solvo)thermal methods

There are various methods for the preparation of nanostructures with different morphology (nanotubes, nanorods, nanowires, nanoribbons, nanoblocks, *etc.*): sol–gel process, electrodeposition, chemical deposition from colloid solutions, hydrothermal and solvothermal deposition, template synthesis, chemical vapour deposition, physical vapour deposition, aerosol pyrolysis, chemical vapour condensation and freeze drying.[63] Particularly TiO_2 NTs are often prepared by anodic oxidation of the titanium substrate with variable anodization parameters [12,64] and by template,[12,65,66] chemical (sol–gel) [67,68] and hydrothermal [69–71] methods. Each method has its own benefits and drawbacks. In this review, the attention is concentrated on the preparation of self-organized one-dimensional structures by simple electrochemical anodic oxidation of titanium metal in an electrolyte solution, which gives an ensemble of nanotubes with a quasiperiodic hexagonal ordering on a substrate, which have a high aspect ratio and a large specific surface area. The method is relatively simple and economically feasible. In addition, this allows easy control of the morphology of an ensemble of nano-

A.A.Rempel. Academician, Doctor of Physics and Mathematics, Director of the Institute of Metallurgy, Ural Branch of the RAS, Head of the Laboratory of High-Entropy Alloys at this Institute, Professor at the Department of Physical Methods and Devices of Non-Destructive Testing of the Institute of Physics and Technology, UrFU.
E-mail: rempel.imet@mail.ru
Current research interests: nonstoichiometry, structural defects, order–disorder phase transitions, quantum size effects, nanomaterials, nanotechnologies.
A.A.Valeeva. Candidate of Chemistry, Leading Researcher at the Laboratory of Nonstoichiometric Compounds of the Institute of Solid State Chemistry, Ural Branch of the RAS, Associate Professor at the Department of Physical Methods and Devices of Non-Destructive Testing of the Institute of Physics and Technology, UrFU.
E-mail: anibla_v@mail.ru
Current research interests: nonstoichiometry and ordering in oxides and oxide nanomaterials, structure and properties of nonstoichiometric oxides.
A.S.Vokhmintsev. Candidate of Physics and Mathematics, Associate Professor at the Department of Physical Methods and Devices of Non-Destructive Testing of the Institute of Physics and Technology, UrFU, Senior Researcher of the NANOTECH Centre, UrFU.
E-mail: a.s.vokhmintsev@urfu.ru
Current research interests: optical materials, memristors, nanostructured compounds
I.A.Weinstein. Doctor of Physics and Mathematics, Professor, Professor of the RAS, Chief Researcher at the NANOTECH Centre, UrFU, Head of the Department of Physical Methods and Devices of Non-Destructive Testing of the Institute of Physics and Technology, UrFU and the Laboratory of High-Entropy Alloys of IMET UrB RAS.
E-mail: i.a.weinstein@urfu.ru
Current research interests: wide-gap nanostructured materials, optical and luminescence spectroscopy, memristive properties of oxide nanostructures.
Translation: Z.P.Svitanko

tubes (aspect ratio, length, inner and outer diameters, distance between nanotubes and the degree of ordering) by varying the principal parameters of the synthesis (temperature, current and voltage, conditions of electrolysis, concentration of ions, pH, time, and titanium foil morphology and composition).

Hoyer [65] reported one of the first studies of the synthesis of TiO_2 NTs, which describes the electrochemical deposition on an ordered alumina template. Immediately after the deposition, the spatial atomic structure of TiO_2 NTs was amorphous. According to transmission electron microscopy (TEM) data, the inner tube diameter was $\sim$100 nm. The active development of methods for the preparation of nanotubes started in the mid-1990s. In particular, template methods were combined with sol – gel and hydro(solvo)thermal methods and with the atomic layer deposition.[12, 72 – 75]

Currently, template method is widely used to prepare TiO_2 nanotubes and nanorods. The template is usually a nanoporous alumina membrane containing an array of parallel rows of nanopores with controlled diameter and length. The structural units of the TiO_2 matrix and the framework are formed around the template. Removal of the template leaves a nanostructure with the same size and shape, *i.e.*, a porous material, nanotubes or wires are formed. Sander *et al.*[74] manufactured dense and ordered TiO_2 nanotubes with a controlled size using the template method. The authors presented a detailed scheme for the preparation of TiO_2 NTs. According to this scheme, first, the template is fabricated by anodization of an aluminium film; then atomic layer deposition of TiO_2 on the template represented by the nanoporous alumina membrane is performed; in the next stage, the upper layer of TiO_2 is removed from the template by mechanical polishing; in the final stage, the template is removed by chemical etching, while TiO_2 NTs remain on the substrate.

The combination of the sol – gel and template method also leads to good results. The sol – gel process belongs to wet chemistry methods; the synthesis is carried out at a slightly elevated temperature, so that the product morphology (size) can be controlled. The essence of the method is to form metal-oxo polymer chains from soluble alkoxides. Metal alkoxides (tetrabutyl titanate or titanium isopropoxide) are normally used as precursors. The synthesis includes hydrolysis and polycondensation reactions, which afford result in the formation of sols. The hydrolysis affords the $TiO_2 \cdot n\,H_2O$ hydroxide gel, which does not contain anions and contains the highest possible amount of water. The dehydration is carried out at moderate temperatures; it is accompanied by the formation of TiO_2 powder with a small particle size (<10 nm), extensive surface area and fairly high reactivity. The pores of the Al_2O_3 template are treated with the resulting TiO_2 sol, the product is heat-treated, and then the template is dissolved.[60, 75] In this method, the size of TiO_2 particles can be controlled owing to the template used.

TiO_2 nanotubes are also prepared using micellar templates comprising appropriate surfactants above the critical micellar concentration. For this purpose, surfactants are aggregated and dispersed in a liquid to form spherical or rod-like micelles, which are used as templates to obtain TiO_2. In this approach, the nanotubes are produced, most often, using water containing cylindrically shaped reverse micelles. The reaction of the titanium precursor (*e.g.*, $TiCl_4$) with the micellar surface and subsequent removal (burning-out) of the surfactant afford a nanotubular structure.

One more widely used technique for the preparation of one-dimensional TiO_2 nanostructures is the hydro(solvo)-thermal process, which was first reported by Kasuga *et al.*[67] The solvothermal and hydrothermal methods are virtually identical; in both methods, TiO_2, $TiCl_4$ or tetrabutyl titanate is used as the precursor. The difference between the methods is only in the solvents used. The hydrothermal synthesis is carried out in aqueous solutions, while the solvothermal process is conducted in organic solvents (ethanol, ethylene glycol, hexane, *etc.*). The temperature of the solvothermal process can be considerably higher than the temperature of the hydrothermal process if the organic solvent boils at a higher temperature than water. Using solvothermal method, it is most often possible to control the size, shape and crystal structure of the resulting nanotubes and nanorods. The solvothermal process is a universal approach to the synthesis of nanomaterials with a narrow size distribution and various degrees of dispersion. The process includes treatment of TiO_2 bulk powders with a NaOH solution in a Teflon-lined autoclave in the temperature range from 100 to 150 °C for several hours with the subsequent treatment with hydrochloric acid.[57]

The formation of nanotubes is based on peeling off the TiO_2 crystal layers in an alkaline medium and stabilization of the $TiONa^+$ complex ion; this gives $[Na_2TiO_3]$ nanosheets, which are rolled into nanotubes during cooling. The morphology of the obtained nanomaterials depends on the process parameters (structure of the precursor, nature and concentration of the alkaline solution, reaction temperature and time); this means that the synthesis of nanostructures is controlled. These tubular structures have several shells (walls), their outer diameter is $\sim$10 nm, and their length varies from several tens to several hundred nanometres. According to TEM studies, the tubular structures have one to five walls separated by <1 nm distances. The inner diameter of the nanotubes ranges from 5 to 6 nm. A drawback of the tubes obtained in this way is that the TiO_2 NT layers are non-uniformly distributed on both sides of the tubes, *e.g.*, there are two layers on one side and three or four layers on the other side.

Maslennikova *et al.*[76] obtained potassium titanate nanotubes by the hydrothermal treatment of two different initial mixtures of metal oxides to precipitate metal hydroxides. According to the first procedure, TiO_2 and dopants were treated in an autoclave with aqueous KOH at temperatures of 170 – 180 and 220 °C and pressures of 1 – 10 MPa; in the second case, hydroxides were precipitated with NH_4OH from mixtures of aqueous solutions of $TiCl_4$ and salts of doping elements; the hydrothermal treatment was carried out in an autoclave at 170 – 180 °C. Under hydrothermal conditions, nanotubes that were stable up to 500 °C crystallized from the precipitated hydroxides. The resulting nanotubes had a high specific surface area (220 – 301 $m^2\ g^{-1}$); their diameter depended on the dopant (Ni, Al, Mg) and varied in the 5 – 11 nm range.

2.2. Electrochemical synthesis, anodization

Titania nanotubes are often synthesized merely by electrochemical anodization. According to this method, the metal is anodized in an electrochemical system, and this initiates the oxidation

$$M \rightarrow M^{n+} + n\,e^- \qquad (1)$$

In an early study [77] of the effect of fluorides on the passivity of the titanium surface carried out in 1979, the

authors found that porous titania layers are formed on the titanium surface at low fluorine concentrations. No TEM examination of the morphology was carried out; therefore, it cannot be stated with confidence that the authors prepared the self-organized TiO_2 NTs. The anodization conditions were gradually altered and optimized as the mechanism of nanotube growth was being clarified. Despite the fact that quantitative measurements of the oxidation and dissolution rates are still impossible, a qualitative understanding of the mechanism of nanotube self-organization has been attained to date.

Anodic oxidation of titanium in an aqueous solution of hydrofluoric acid in the presence of chromium(VI) ions was first studied in detail and described back in 1999 by Zwilling *et al.*[51] The authors proposed the growth mechanism for a dense TiO_2 NT film on the surface of the titanium foil and TA6V aluminium/titanium/vanadium alloy. The mechanism includes competition between titanium dissolution and titanium oxide formation, with the chromium(VI) ions being the poison and fluoride ions being the antidote. The result of this competition is the growth of the porous film with a regular tubular structure, which does not stop for a long period of time. Finally, a steady state with continuous consumption of the anodic current is established.

Denisenko *et al.*[78] revealed the effect of the water concentration in the fluoride solution on the geometric characteristics of the obtained coatings and TiO_2 NT morphology. The change in the fluoride ion activity in the electrolyte caused by the increase in the water concentration from 2 to 10 mass % leads to a decrease in the nanotube length from 100 to 4 μm and increase in the nanotube inner diameter from 114 to 270 nm, *i.e.*, the aspect ratio changes.

Roy *et al.*[12] pointed out that, depending on the type of electrolyte and anodization parameters, the following cases are possible:

— M^{n+} ions are solvated in the electrolyte; the metal is continuously dissolved (corrosion or electropolishing);

— M^{n+} ions react with O^{2-} ions (oxygen comes from water); if the formed oxide is insoluble in the electrolyte, then a compact oxide layer is formed on the metal surface;

— two competing processes — solvation and oxide formation — afford highly ordered nanotubes or nanopores;

— fast growth of nanotubes of various lengths (up to 100 μm) randomly arranged in space takes place; if the nanotubes grow in bundles, they are poorly attached to the substrate;

— formation of thick self-organized mesoporous layers.

To date, five generations of TiO_2 NTs have been obtained by electrochemical oxidation. The first-generation nanotubes were synthesized by Zwilling and *et al.*[79] by anodization. The authors obtained self-organized TiO_2 NTs arranged perpendicular to the titanium substrate. They used the chromic acid electrolyte without addition of hydrofluoric acid and in the presence of hydrofluoric acid (0.5 mass % HF). The resulting nanotubes had a length of 200–500 nm, a diameter of 10–100 nm and a wall thickness of 13–27 nm; the spatial atomic structure was disordered and the side walls were non-uniform due to fluctuations of the anode current.

The length of the second-generation TiO_2 NTs was increased to 2.4 μm by varying the pH of the fluoride-containing buffer electrolyte;[80] the nanotube diameter reached 100 nm and the wall thickness was up to 12 nm. The hydrofluoric acid was replaced by a fluoride salt [1 M $Na_2SO_4/(NH_4)_2SO_4$ + 0.5 mass % NH_4F]; therefore, the TiO_2 dissolution rate decreased, which resulted in increasing film thickness on the titanium foil surface. According to Macak *et al.*,[80] lower pH level in the lower part of nanotubes is a direct consequence of the anodic oxidation of titanium with water, which consumes oxygen atoms and leaves a medium with a high H^+ concentration. This accelerates thinning of the barrier layer at the metal/oxide interface. The reactions in the bottom part of nanotubes virtually preclude the quantitative estimation of the pH change.

The third-generation nanotubes were synthesized using a fluoride-containing organic electrolyte: 0.5 mass % NH_4F + 2 vol.% H_2O in ethylene glycol.[26,81,82] The use of this electrolyte led to lower rate of dissolution of the oxide layer; this afforded smooth nanotubes with a high aspect ratio; the nanotube length varied from 5 μm to 1 mm, the diameter was 100 nm and the wall thickness reached 12 nm. According to Grimes and coworkers,[83] the metal corrosion was enhanced when a polar organic electrolyte was used, while the presence of large cations in the fluorides increased the barrier layer at the metal/oxide interface.

The fourth-generation nanotubes were obtained with fluorine-free electrolytes. Fast anodization resulted in the generation of nanotubes with aspect ratios varying over wide ranges and various morphologies. The synthesis using electrolytes based on oxalic, hydrochloric and sulfuric acids yielded disordered bundles of nanotubes. When oxalic acid was used, the nanotubes were found to contain considerable amounts of carbon. Hahn *et al.*[84] used a chlorine-containing electrolyte (0.01–3 M $HClO_4$) to synthesize randomly arranged 30 μm long nanotubes with diameters ranging from 20 to 40 nm and wall thickness of 10 nm.

The five-generation nanotubes were prepared by multistage anodization in organic electrolytes containing fluoride ions (0.5 mass % NH_4F + 2 vol % H_2O in ethylene glycol). This gave smooth hexagonal nanotubes with a length from 2 to 10 μm and a diameter of 100 nm; the wall thickness reached 15–20 nm.[85,86]

To date, numerous studies have been carried out to establish the relationship between the physicochemical parameters of synthesis and the structure, properties and geometric characteristics of TiO_2 NTs. The results of these studies are different; the differences were attributed to the application of various electrolytes and to different morphology (composition) of the titanium foil.[87–98] When the anodic oxidation was carried out using a fluorine salt, impurities appeared on the TiO_2 NT surface because of the hydrolysis of $[TiF_6]^{2-}$. The impurity layer plugged the open part of the nanotubes, which hampered the diffusion of reactants and changed the physical properties. It was found that in electrolytes with pH < 3, smaller amount of impurity products was formed on the nanotube surface, but under these conditions, the nanotube length was restricted due to the high activity of fluoride ions.[88] The increase in the anodization time resulted in the formation of a clean surface.[89] As the process temperature and the concentration of water in the organic electrolyte increased, the rate of the chemical dissolution increased, which gave a clean surface.[90,91] Pridaa *et al.*[92] proposed washing of TiO_2 NTs after anodization with methanol to completely remove impurities from the surface.

Thus, the anodic oxidation allows one to control the morphology (nanotube length and inner and outer diame-

ters) and the structure of the obtained TiO_2 NTs by varying the parameters of synthesis (electrolyte composition, content of water, pH of the medium, current density and voltage, anodization time and temperature and multistage character of the process). Currently, it is possible to fabricate coatings of titanium dioxide nanotubes with different morphologies, structures and propertie for solving particular problems.

3. Structure

3.1. Atomic structure

There are various crystalline polymorphs of titanium dioxide: anatase, rutile, brookite and so on. The synthesis by anodic oxidation gives mainly amorphous TiO_2 NT structures. Some publications (*e.g.*, Refs 99–101) indicate the presence of a crystalline phase in nanotube walls after anodization at high anode voltages. In addition, anodization in acidic medium (H_2SO_4) can also give a film consisting of anatase crystal phase, an anatase + rutile mixture or rutile crystals, depending on the anodization conditions (spark, potentiostatic or galvanostatic process).

The amorphous nanotube film on the titanium surface consists of a continuous thin barrier layer adjoining the metal and a porous outer layer. The TiO_2 nanotubes are formed in several stages (Fig. 1).[12, 102] In the first stage, the titanium oxide film on the foil surface is thickened, which causes a drop of the anodic current. Under the action of the applied voltage, water dissociation takes place at the electrolyte/oxide interface

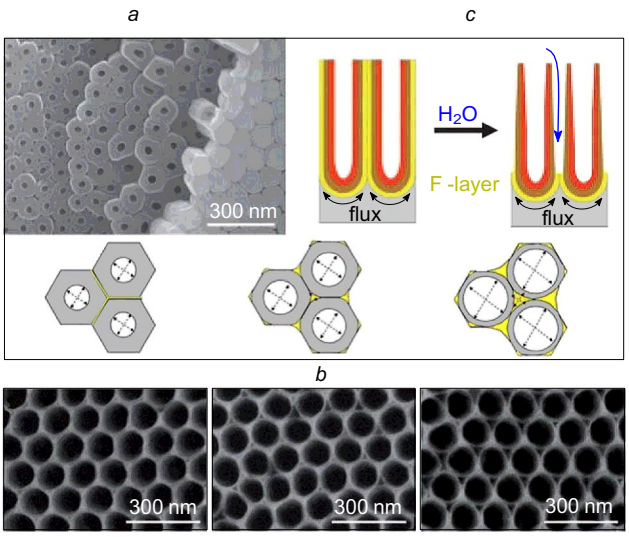


Figure 1. Formation of TiO_2 NTs from a porous layer.[12] (*a*) Scanning electron microscopy illustration of pore formation; the image was taken through the bottom of the nanotubular layer detached from the metal substrate at a small angle; the lower part of the tubular layer is only a close-packed hexagonal porous layer gradually transformed into round tubes; (*b*) transition from a porous to a tubular structure (from left to right); (*c*) graphical presentation of the formation of tubular morphology from the initially porous morphology *via* selective dissolution of fluoride-rich layers and predominant etching of the triple points with aqueous electrolyte; the red-brown colour marks titanium dioxide, yellow colour indicates a fluorine-rich titanium dioxide layer and gray designates metallic titanium. Published with permission from Wiley and Sons.

$$H_2O \rightarrow 2H^+ + O^{2-} \quad (2)$$

and the oxygen ions migrate towards the metal/oxide interface where they react to give intermediate oxides

$$Ti + xO^{2-} \rightarrow TiO_x + 2xe^- \ (0.5 < x < 2) \quad (3)$$

It is noteworthy that movement of the Ti^{4+} ions in the barrier layer towards the oxide/electrolyte interface is slow and is restricted by excess titanium in the film. Thus, the kinetics of anodic oxidation is determined by the O^{2-} diffusion in the barrier layer. The concentration gradient of the oxygen ions results in the formation of various non-stoichiometric titanium oxides ($TiO_{0.9-1.1}$, Ti_2O_3, Ti_3O_5, Ti_4O_7, Ti_6O_{11}, Ti_7O_{13}, Ti_8O_{15}, Ti_9O_{17}, $Ti_{10}O_{19}$, TiO_2). At the same time, hydrogen is reduced at the cathode

$$2H^+ + 2e^- \rightarrow H_2\uparrow \quad (4)$$

In the second stage, pores are formed in the resulting TiO_2 film. This can be attributed to the non-uniform distribution of the electric field on its surface. The non-uniformity induces the tendency of the fluoride ions to migrate from electrolyte towards the TiO_2 film, which brings about local destruction of the oxide and gives rise to pits, which subsequently act as pore-forming centres. In addition, as the pores grow (the active surface area increases), the current increases. The chemical reaction of titanium oxide dissolution gives a water-soluble hexafluorotitanate(IV)

$$TiO_2 + 4H^+ + 6F^- \rightarrow [TiF_6]^{2-} + 2H_2O \quad (5)$$

In parallel, continuous oxidation at the titanium/oxide interface takes place. As a rule, adjacent pores are expanded simultaneously until the electrically conductive titanium phase between them is oxidized. In the third stage, the current decreases and a permanent phase is formed. During this period, the pores grow in depth *via* permanent displacement of the barrier layer, which retains its thickness.

It is noteworthy that the key role of fluorides is to maintain a thinner bottom oxide layer[103] by chemical etching of the oxide layer and the complex formation of Ti^{4+} ions that enter the electrolyte. One more important factor is that the fluoride ions have a small radius and compete with O^{2-} for migration across the TiO_2 barrier layer; the migration rate of fluoride ions is $\sim$2 times higher than the migration rate of the oxygen ions. Consequently, a fluorine-rich layer is formed at the metal/oxide interface and then at the pore boundaries.[100] Fluorine compounds are water-soluble; therefore, gradual etching out of the pore boundary takes place, resulting in the formation of tubes. The growth of nanotubes is terminated when the equilibrium is attained between the rates of nanotube formation (downward displacement of the tube bottom) and thinning of the tube tips.

Thus, the synthesized TiO_2 NTs are amorphous; the morphology of the resulting films depends on the kinetics and conditions of the electrochemical process; by varying the parameters of synthesis, it is possible to obtain either ordered nanotubes and pores or disordered nanotube bundles.

3.2. Electronic structure, nonstoichiometry

Titanium dioxide is an n-type semiconductor with a wide band gap (3.0–3.3 eV), the size of which depends on the particular polymorph. Stoichiometric TiO_2 is transparent in the visible spectral range and absorbs UV radiation. An

efficient way for variation of the atomic and electronic structures of TiO_2 is to change its stoichiometry by generating structural vacancies in the oxygen sublattice; this shifts the spectral response to the visible region of the electromagnetic radiation spectrum and decreases the band gap.[34–37]

Valeeva *et al.*[34, 35] carried out anodization of a 100 μm-thick titanium foil in an electrochemical cell maintained in a thermostat at 20 °C on a Digma setup. TiO_2 NTs were formed in a fluorine-containing solution of ethylene glycol (1 mass % NH_4F) in the potentiostatic mode (U = 20 V), with anodization time (t_a) ranging from 15 to 360 min. It was established that the anodization time and parameters (voltage, current), properties of electrolyte (concentration, temperature) and the foil surface affect the morphology and properties of the resulting nanotubes. The process gave TiO_2 nanotubes with a length (L) from 550 nm to 1.5 μm, inner diameter ranging from 27 to 39 nm and outer diameter of 42 to 53 nm. It was shown that with increasing anodization time, the solid fraction (A) decreased from 0.39 to 0.25. The greatest L = 1.5 μm and effective surface area S_{eff} = 415 cm^2 for the nanotubes were attained at t_a = 120 min. At a certain time point during anodization, a decrease in the current density was noted, resulting in decreasing growth rate of the oxide layer and, consequently, in acceleration of its dissolution. The X-ray diffraction pattern of TiO_2 NTs showed an intense diffuse halo at small angles (18 to 38°) and no diffraction peaks, which confirmed that the obtained titanium dioxide was amorphous. A dip was found in visible range of the experimental diffuse reflectance spectra of TiO_2 NTs, caused by atomic defects in the amorphous network. The presence of structural vacancies brings about visible absorption due to the formation of allowed states in the TiO_2 band gap. In addition, the X-ray photoelectron spectrum of the amorphous NT film showed an additional doublet corresponding to the Ti^{3+} ion.

The energy band diagram of TiO_2 NTs is presented in Fig. 2. The impurity levels are electron acceptors, the band gap of stoichiometric TiO_2 is ~3.3 eV, while that of non-stoichiometric titanium oxide (TiO_{2-x}) is ~2.8 eV. Thus, the presence of atomic defects, particularly, oxygen vacancies, in the crystal lattice leads to more efficient absorption of visible light (owing to a decrease in the effective band gap) and, hence, to an increase in the catalytic activity of the film.

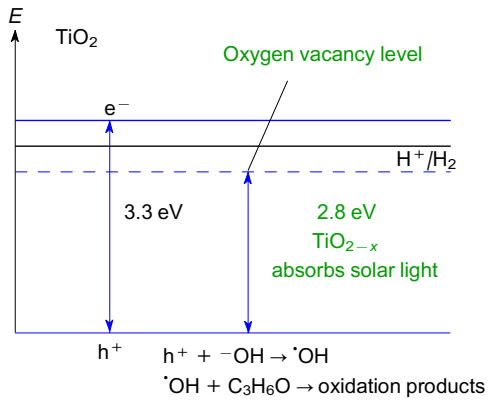


Figure 2. Diagram of the electronic band structure of TiO_2 NTs with oxygen vacancies. The energy values in electronvolts (eV) are referred to the standard hydrogen electrode potential. The figure was compiled by the authors on the basis of published data.[34]

3.3. Modification of structure and phase composition

Materials with specific electrical, optical or chemical properties required for some applications are created by modification of nanotubes. Currently, the following methods are mainly used to modify TiO_2 NTs:

— heat treatment, which changes the type and ratio of crystal phases, the conductivity and the charge carrier lifetime;

— doping with cations and anions to enhance the light absorption and prevent electron (hole) recombination;

— decoration and fabrication of semiconductor heterostructures, which ensure optimal energy levels for charge absorption and separation.

The heat treatment of amorphous nanotubes synthesized by anodization is usually carried out in air or in a gas medium (N_2, O_2 or N_2+H_2 mixture). This is accompanied by a change in the shape, non-stoichiometry, phase composition and properties of nanotubular materials.[34, 35, 104, 105] The point defects in the crystal lattice lead to a change in the optical and photocatalytic properties of the materials. According to Chen and co-workers,[106, 107] titanium oxides with different valence are formed in the oxide layer after high-temperature treatment. The authors proved for the first time the presence of oxygen vacancies in the anodized nanotubular TiO_2 structures (Fig. 3). Later, a noticeable concentration of Ti^{3+} and a lower concentration of Ti^{2+}, were detected by X-ray photoelectron spectroscopy (XPS),[108] apart from Ti^{4+} ions, in the samples obtained by anodization in a solution containing 0.3–2.4 M H_2O and 0.015–0.17 M NH_4F. A study dealing with the effect of H_2O and NH_4F contents in the electrolyte on the morphology and properties of the TiO_2 barrier layer[109] demonstrated that an increase in the concentration of NH_4F from 0.05 to 0.2 M results in higher contents of Ti^{3+} and Ti^{2+} ions in the layer of TiO_2 nanotubes synthesized in the potentiostatic mode. The Ti^{3+} and Ti^{2+} concentrations in the film decreased when the water content in the electrolyte during the nanotube synthesis was 1 to 50%. The morphology of the synthesized nanotubes also influenced the structure and phase composition of TiO_2 NTs.

It was shown[110] that the surface area to volume ratio of TiO_2 NTs increased with decreasing diameter of the nanotubes, which resulted in the formation of a larger amount of Ti^{3+} ions and oxygen vacancies during the high-temperature annealing.

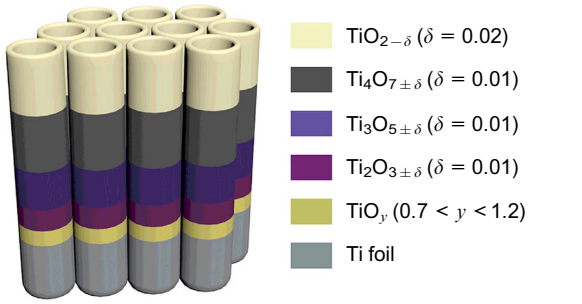


Figure 3. Schematic view of TiO_2 layers of various stoichiometry formed in titanium foil. The figure was created by the authors using published data.[106]

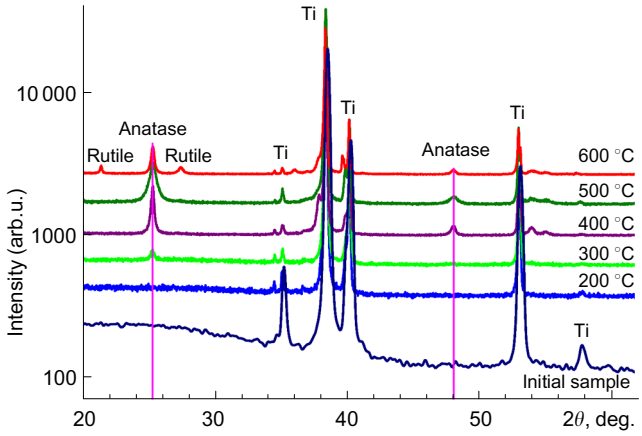


Figure 4. X-ray diffraction patterns of the TiO_2 nanotubular films annealed in air at different temperatures.[35] Published with permission from Elsevier.

According to the results of Valeeva *et al.*,[35] annealing of NT films in air in the temperature range of 200–600 °C for 1 h is accompanied by phase transitions: the initial amorphous phase is transformed into anatase at 300 °C, while the annealing at temperatures above 500 °C gives rise to rutile (Fig. 4). At temperatures $\geqslant$500 °C, the surface morphology of nanotubes changes: tubes are broken and a part of the surface is sintered to give the compact oxide, which reduces the effective surface area. Analysis of the XPS spectra of the TiO_2 nanotubes annealed at 600 °C revealed an additional $Ti2p_{3/2}-Ti2p_{1/2}$ doublet with the $Ti2p_{3/2}$ binding energy of 457.5 eV (the binding energy values correspond to the Ti^{3+} ion) and impurity peaks at 532.2 and 533.6 eV, which refer to the carbon- and nitrogen-containing surface impurities and OH groups.

The atomic ratios of elements in the near-surface layer of the photocatalysts depend on the heat treatment conditions. The heat treatment at 300–500 °C leads to increasing $[O_{Ti}]:[Ti]$ ratio, and only Ti^{4+} ions are present in the films.

According to Ghicov *et al.*,[111] a pronounced conversion of nanotube layers to anatase starts at ~280 °C, while the formation of the rutile phase starts above 500 °C. Further increase in the annealing temperature leads to a change in the ratio of the anatase and rutile phases: 12-hour annealing in air gives 4% rutile at 500 °C, 17% at 600 °C, 30% at 700 °C and 46% at 800 °C; the annealing at 900 °C for two hours with temperature rise at a rate of 1 °C s^{-1} gives the rutile phase alone. In addition, nanotubes contain a considerable amount of fluoride ions, carbon and surface hydroxyl groups. It was shown that after usual heat treatment, the fraction of titanium in the Ti^{3+} state is 1%. The annealing in different gas media (such as air, N_2, O_2 or a N_2+H_2 mixture) leads to different ratios of the anatase and rutile phases.[12] Thus, the duration and the medium of annealing and the rate of temperature rise considerably affect the TiO_2 crystal structure, the ratio of phases and the morphology and composition of the nanotubes.

Currently, doping is the most promising method for modification of TiO_2 NTs. Doping is carried out by substituting Ti^{4+} ion sites with rare earth, noble or transition metal cations and substituting oxygen sites with carbon, sulfur, fluorine, nitrogen and other anions. Doping with cations narrows down the band gap of TiO_2 *via* the formation of additional levels, which change the quantum efficiency of titanium dioxide, the recombination rate of photogenerated charge carriers and the photocatalytic activity.[112–119] It was shown[120] that the photocatalytic activity of TiO_2 depends on the concentration and sort of the cation (In^{3+}, Zn^{2+}, W^{6+}, Nb^{5+}, Li^{+}, *etc.*); doping induces a red shift of the absorption spectrum, which does not always indicate an increase in the photocatalytic activity. In addition, modification of nanotubes results in increase in the electrical conductivity; the type of conduction depends on the oxidation state of the doping metal. When TiO_2 NTs are doped with cations in a high oxidation state, *e.g.*, Nb^{5+}, the conductivity increases due to the transfer of electrons to the conduction band; in this case, n-type conduction is observed.[121] When doping cations occur in a lower oxidation state, *e.g.*, Fe^{3+}, the conductivity increases *via* the transfer of electrons from the conduction band to generate holes; in this case, conduction is of the p-type.[122] The cation doping of TiO_2 NTs gives rise to defects, which can serve as charge recombination centres; when recombination predominates, the photocatalytic activity of TiO_2 NTs decreases.

According to several studies,[123–127] anion doping brings about better results than the use of cations. Doping with anions (nitrogen-, sulfur-, carbon-, phosphorus- and boron-containing ones) generates less recombination centres and gives rise to absorption bands adjoining the visible range, which increases the photocatalytic activity, especially in the case of carbon and nitrogen doping.[128, 129] When TiO_2 NTs are doped with carbon, the band gap decreases and the absorption spectrum shifts due to the formation of stable impurity levels above the energy levels of the TiO_2 valence band;[130] in addition, the surface carbon compounds act as centres of absorption of visible radiation. The most popular method for the shift of the absorption spectrum to the visible range is to insert nitrogen into oxygen sites or into the lattice interstices.[131] In the former case, a new level appears above the ceiling of the TiO_2 valence band, while in the latter case, a new level 0.76 eV higher than the valence band is formed. Nitrogen doping of TiO_2 NTs extends the absorption range towards the visible region, increases the photocatalytic activity and changes the optical, mechanical and electrical properties. It was shown[132] that the introduction of fluoride ions into TiO_2 promotes conversion of Ti^{4+} to Ti^{3+} and generation of oxygen vacancies. A moderate shift of absorption to longer wavelengths takes place and the photocatalytic activity increases *via* decrease in the electron and hole recombination at a certain concentration of Ti^{3+} ions.

3.4. Modification of functional properties

As noted above, TiO_2 NTs obtained by anodic oxidation are either amorphous or partly contain crystal phases of anatase, anatase + rutile mixture or rutile, depending on the conditions of anodization. Modification of the amorphous structure induces changes in the properties; modification methods are considered above (see Section 3.3). The properties of TiO_2 NTs depend mainly on the bulk and surface structural defects, in particular, on the formation of titanium in low oxidation states (Ti^{3+}, Ti^{2+} and Ti^{+}) and oxygen vacancies. Structural defects appear upon annealing in vacuum or in inert atmosphere. Annealing in air induces transition of TiO_2 from the amorphous to crystalline state, namely, to anatase when annealing is conducted in the temperature range of ~280–500 °C and to rutile in the

case of annealing above 500 °C. It should be noted that the temperature of each transition depends on the geometric parameters, the nature of the dopants and the impurities that may be present in TiO_2 NTs.[133–135] Long-term annealing at 500 °C does not change the TiO_2 NT morphology, but at higher temperatures, degradation of nanotubes takes place.

The formation of Ti^{3+} in the near-surface layer of TiO_2 NTs accounts for the enhanced conductivity and visible absorption. This is due to the formation of additional energy levels or a high density of localized donor states (Ti^{3+}, which is an electron donor, is located near the conduction band of TiO_2). The change in the electronic structure brings about a decrease in the effective band gap and a shift of the absorption spectrum to the visible region, which, in turn, leads to a considerable increase in the photocatalytic activity of titanium dioxide in the oxidation of organic molecules and hydrogen evolution from aqueous solutions.

Apart from defects, the photocatalytic and sorption properties of TiO_2 are considerably affected by its surface and structure. It was ascertained that the specific surface area is important for heterogeneous catalysis: the larger the specific surface area, the higher the yield of the reaction product.[136] The efficiency of photocatalysis is also influenced by the TiO_2 structure (anatase or rutile). It was noted[137,138] that rutile with less extensive surface area is more efficient than anatase with a larger specific surface area.

It was shown[34] that the element atomic ratios in the near-surface layer of the photocatalysts depend on the annealing temperature. According to XPS data, the synthesized amorphous film and the films annealed at 600 °C contain Ti^{3+} ions. The annealing at temperatures of 300–500 °C leads to increasing $[O_{Ti}]:[Ti]$ ratio, and the films contain only Ti^{4+} ions. Changes in the structure, nonstoichiometry and phase ratio lead to modification of the TiO_2 NT properties. The film annealing in the temperature range of 200–600 °C decreases the band gap from 3.3 to 3.0 eV. In addition, the photocatalytic activity of TiO_2 NTs increases at 500 °C owing to the formation of the anatase phase, high defectiveness of the structures and extensive surface area. It was found experimentally that the photocatalytic activity of TiO_2 NTs in the photo-oxidation of acetone under visible light irradiation is 3–4 times higher than that of the commercial catalyst Degussa P25. Earlier, similar results were observed by Macak *et al.*[139] in the photocatalytic oxidation of the AO7 dye in an aqueous solution under UV irradiation at 325 nm. The highest activity was found for the nanotubes annealed at 450 °C and containing only the anatase TiO_2 phase. It was noted that in the presence of even a minor quantity of rutile (annealing temperature of 550 °C), the decomposition rate of AO7 considerably decreased. Liang and Li[140] reported that the sample representing an anatase and rutile mixture, conversely, showed high photocatalytic performance towards degradation of 2,3-dichlorophenol in an aqueous solution under UV irradiation. It is known that anatase has a higher photocatalytic activity than rutile, although rutile has a smaller band gap (3.2 eV for anatase and 3.0 eV for rutile) and, hence, a better response in the visible region should be expected. However, the e^-/h^+ pair recombination is faster in rutile;[141] this decreases the photocatalytic activity.

Thus, a change in the crystal structure and formation of the defective structure of TiO_2 NTs are efficient methods for increasing the photocatalyst activity in the visible region.

4. Applications

4.1. Heterogeneous photocatalysis

Heterogeneous photocatalysis is an available and reliable technology. It is a cheap and robust method for water and air purification from organic and inorganic compounds (including heavy metals) and for CO_2 and steam conversion to hydrocarbon fuel. In recent years, considerable attention has been paid to green chemistry, in particular, to the use of photocatalysis for the oxidation of toxic organic pollutants in waste water to harmless carbon dioxide and pure water. The essence of the photocatalytic oxidation of organic compounds is as follows: on exposure to light, excitons are formed in titanium dioxide nanoparticles; over a short period of time, excitons decay into holes and excited electrons. Holes diffuse to the particle surface and then interact with an electron donor in the solution or with hydroxide ions to give strong oxidants, *e.g.*, hydroxyl or superoxide radicals. The conduction electrons, after diffusion to the TiO_2 surface, interact with oxygen molecules; this gives superoxide radical anions $O_2^{-\bullet}$. The electrons can also interact with organic solvents (electron acceptors). The formation of electrons and holes makes the TiO_2 surface a highly potent oxidant; therefore, pollutants can be mineralized *via* photocatalytic destruction to H_2O and CO_2.

The completion of reactions and high quantum activity of the photocatalyst are affected by catalyst characteristics such as porous morphology and defective crystal structure, specific surface area, the size of band gap, the number of active sites and excited state lifetimes for electrons and holes. A high-performance photocatalyst may have a band gap not exceeding 3 eV. In this case, the energy of visible-light photons is sufficient for absorption and photoactivation of the photocatalyst. Quenching of the radiative recombination in the electron – hole subsystem of the photocatalyst additionally increases the catalytic activity and the yield of the useful reaction products. Thus, high-performance semiconductor nano-photocatalysts should meet the following requirements: they should be nanostructured (and have a high specific surface area), absorb visible light and have a specified size of the band gap, high concentration of active sites, long lifetime of the electron excited state, and also have homo- or heterojunctions for efficient separation of photon-excited electrons and holes and their delivery to the surface. Furthermore, conditions for the formation of free radicals should exist on the catalyst surface.

Titania-based photocatalysts are usually obtained as powders, which complicates their practical application. It is most appropriate to form membranes and coatings, since in this case, there are no problems associated with isolation of the powder from the suspension (if the catalysis is conducted in the liquid medium) or illumination of the catalyst (in the case of gas-phase catalysis). In addition, nanotubular films with cylindrical pores of a specified diameter, which are strictly perpendicular to the surface, are compact and can be used in places inaccessible for solar light when combined with light-emitting diodes. This markedly increases the potential of TiO_2 nanotubes in catalysis.

The fabrication of semiconductor heterostructures is a new approach used to increase the catalytic activity of TiO_2 NT-based catalysts. The nanotubes are decorated with semiconductors such as CdS, CdTe, PbS or Cu_2O.[142–144] The heterostructures consisting of several semiconductor particles are active under visible light; owing to a high degree of charge separation, they have a pronounced photocatalytic activity.[145–149] A narrow band gap semiconductor with a more negative conductivity level compared to TiO_2 acts as a visible-light sensitizer for TiO_2. The effective electron transfer between TiO_2 and the sensitizer takes place when the titania conduction band has a more positive potential than this band of the sensitizing semiconductor. Visible light irradiation of the heterostructure leads to generation of charge carriers only in the sensitizer; as this takes place, excited electrons migrate to the TiO_2 conduction band. If the valence band of the sensitizer is located above the ceiling of the TiO_2 valence band, the holes generated in the sensitizer valence band remain there.

A recent practical study dealt with increasing the TiO_2 NT activity by using cadmium sulfide, a known semiconductor with an energy gap of $\sim$2.4 eV.[39] In this study, TiO_2 nanotubes were decorated with CdS nanoparticles synthesized by chemical condensation in an aqueous solution and wiyj TiO_2 nanoparticles synthesized by sol – gel process. Higher photocatalytic activity (in comparison with commercial photocatalysts) was found for the hybrid materials based on TiO_2 NTs decorated with CdS nanoparticles in the oxidation of organic molecules on visible light irradiation: depending on the decoration method, hybrid materials showed a photocatalytic activity of 7 – 20 $\mu mol\,min^{-1}\,g^{-1}$, whereas the activities of the Hombifine and Degussa P25 catalysts were 1 and 3 $\mu mol\,min^{-1}\,g^{-1}$, respectively. Optical and XPS studies and quantum chemical analysis of homo- and heterojunctions made it possible to substantiate the mechanism of activity of the developed hybrid material. This mechanism includes visible light absorption by CdS nanoparticles, excited electron transfer from the CdS conduction band to the TiO_2 conduction band, charge separation (owing to the presence of the heterojunction) and suppression of the band-to-band recombination of the excited electrons and holes. Measurement of the kinetic curves of the catalytic activity showed high temporal stability of the developed hybrid photocatalyst. High stability of the photocatalyst is attributable to successful encapsulation of cadmium sulfide nanoparticles in the TiO_2 NTs protected from the surroundings.

4.2. Nanoelectronics, memristors

Currently, resistive switching processes in anodized TiO_2 layers[150–152] and in TiO_2 NTs[153–160] are being actively studied in order to design new non-volatile memory cells, or memristors, and logical units and artificial neural networks based on them. It is known that the resistive switching in an TiO_2 layer, which underlies the operation of memory storage devices, occurs *via* conductive channels (filaments) composed of oxygen vacancies (V_O) (Refs 150, 151, 153 – 158, 160) or metal ions[152, 159] that are formed in the memristor active layer as a control voltage of appropriate polarity is applied to its electrodes. The primary electroforming of conductive channels is, most often, a necessary stage; this results in transition of the memristor cell from the high-resistance (HRS) to low-resistance (LRS) state, or from the switched off to the switched on state. Then, upon the application of control voltage, the conductive channels are partially destroyed or restored. The reversible LRS $\rightleftarrows$ HRS switching of TiO_2 NT-based memristors occurs exactly in this way, usually in the bipolar mode.[150–160] Meanwhile, Hazra *et al.*[160] demonstrated the possibility of reversible resistive switching without the primary electroforming of conductive channels. The calcination of TiO_2 NTs in air results in a decrease in the concentration of oxygen vacancies in the active layer and degradation of resistive switching parameters,[150, 154, 157] and in some cases, in full loss of memristive properties.[150]

Yoo *et al.*[154] reported a study of the resistive switching effect in the Ti/NT TiO_2/Pt sandwich structure. The TiO_2 NT array was obtained by anodization of a titanium foil in 3 M $HF + H_3PO_4$ electrolyte for 2 h and consisted of 200 nm-long nanotubes of 80 nm diameter. The authors indicated that the V-shape of the obtained nanotubes was perfect for plasma-assisted deposition of a Pt electrode in their cavity. The primary electroforming of conductive channels from V_O was effected by applying a negative voltage on the Pt electrode relative to the grounded Ti electrode. For these memristors, the resistance ratios $R_{HRS}/R_{LRS} > 14$ and the number of complete cycles of resistive switching $N > 20$ were found.

Liu *et al.*[155] showed the possibility of pulsed cathodic electrodeposition of Ag, Cu, Au and Pt into TiO_2 nanotubes, which were completely filled with the metal (M) and fabrication of bulk interdigitated electrodes, specifically for the formation of diverse memristive devices with the Ti/NT TiO_2/M structure. The initial arrays of TiO_2 nanotubes were synthesized by anodization of titanium foil in ethylene glycol with addition of NH_4F and deionized water and consisted of nanotubes with a length of 3 μm and a diameter of 80 nm. The authors of that study additionally annealed the ready Ti/NT TiO_2/M memristor structures in a reductive atmosphere (10% H_2 in argon) at 400 °C for > 12 h. As stated by the authors, this heat treatment resulted in generation of additional oxygen vacancies and improved the resistive switching parameters.

A variety of methods are known for improving the characteristics of memristors based on TiO_2 NT arrays. First, conditions for the electrochemical oxidation are selected to obtain an anodized TiO_2 layer with the optimal thickness and oxygen nonstoichiomety.[150–152, 156, 158] In this case, the electrolyte composition is changed, particularly, glycerol,[150] ethylene glycol,[152, 156–158, 160] orthophosphoric acid[151, 154] or their mixtures[155, 159] are used as the base, and fluoride ions and water are added. The anodization time is varied from several seconds to tens of minutes[150–152, 155, 157, 158] or even to several hours.[154, 156, 159, 160] The anodization voltage is increased from 5 V to several tens of volts,[150–152, 155] and anodization is also carried out at 50,[160] 60,[152, 157] 80 (Ref. 159) and 120 V.[156] For example, Vokhmintsev[156] studied memristors with the Ti/NT TiO_2/Au structure. The initial TiO_2 NTs were synthesized by anodization of titanium foil in ethylene glycol with the addition of 0.05 M NH_4F and had a length of 500 nm and a diameter of 60 nm. The memristors were shown to operate for 15 – 20 complete switching cycles with the resistance ratio $R_{HRS}/R_{LRS} > 50$.

Second, in order to improve characteristics of memristors based on TiO_2 NTs, deposition of metals [*e.g.*, Ag (Ref. 152) and Cu (Ref. 159)] into TiO_2 nanotubes for electroforming of conductive metal channels is carried out.

By anodization of titanium foil in an electrolyte based on ethylene glycol containing 3 vol.% H_3PO_4, 3 vol.% H_2O and 0.5 mass % NH_4F at a constant voltage of 80 V for two hours at room temperature, Chen *et al.*[159] prepared TiO_2 NTs, which were additionally annealed at 500 °C for 1 h to obtain the anatase phase. Copper was electrodeposited into the cavities of these nanotubes. This resulted in copper nanowires (Cu-nw) with a length of 5 μm and a diameter of 100 nm formed inside the TiO_2 nanotubes. The primary electroforming of the conductive Cu channels in an TiO_2 layer was implemented by applying a positive control voltage on the Cu-nw electrodes relative to the grounded Ti electrode. Measurement of the current–voltage characteristics of the Ti/NT TiO_2/Cu-nw/Au memristors showed that the resistance ratio $R_{HRS}/R_{LRS} > 40$ was retained over 10^3 complete cycles of resistive switching. The authors noted that the memristors were operable even after 10^4 switching cycles in the pulsed mode and remained in the corresponding resistive state for $> 10^4$ s.

Third, to improve the memristor characteristics, conductive polymer coatings are formed on the surface and inside of the TiO_2 NTs; this improved the transport of electrons, enhances the stability and increases the service life of the memristor structures. For example, Conti *et al.*[157] investigated the effect of the 40 nm-thick polyacrylic acid (PAA) coating formed by chemical vapour deposition on a layer of amorphous TiO_2 NTs annealed in air at 450 °C for an hour. A 250 nm-thick memristor active layer was synthesized in an electrolyte based on ethylene glycol containing 2.5 vol.% H_2O and 0.5 mass % NH_4F at a constant voltage of 60 V for 30 s and consisted of nanotubes with the outer and inner diameters of 120 and 50 nm, respectively. An increase in the R_{HRS}/R_{LRS} ratio from 2 to 5 and an increase in the number of complete cycles of resistive switching of memristors from 10 to 20 was detected for the Ti/NT TiO_2/Pt and Ti/NT TiO_2/PAA/Pt sandwich structures.

The conductivity mechanisms of the memristor structures were considered.[154, 157] It was found that before electroforming, the Schottky emission predominates both for positive and negative polarity of the control voltage.[157] After the electroforming in the LRS state, the memristor conductivity obeys the Ohm's law, while in the HRS state, Schottky emission [154] or conductivity limited by the spatial charge [157] predominates. Thus, the formation of conductive channels in the active layer of TiO_2 NTs leads to shunting of the Schottky barrier at the M/TiO_2 NT interface. The characteristics of memristor structures based on titanium dioxide films and TiO_2 NT functional layers according to the results of independent studies [150 – 164] are summarized in Table 1 in the chronological order. It can be seen that, according to most of reported data, the memristive behaviour of the prepared layered structures is provided by oxygen vacancies, which form the conducting filaments *via* switching between low- and high-resistance states.

4.3. Power engineering, betavoltaics

Nanostructured TiO_2 is used in the production of photovoltaic cells as photoanode materials.[56, 165 – 168] Quite a few studies in the field of renewable power engineering are devoted to light-sensitized solar batteries based on TiO_2 NTs with energy conversion efficiency of up to 10%.[169 – 176] Hwang *et al.*[177] considered the use of β-radiation of the radioactive carbon isotope for improving the performance of these batteries. In recent years, scientists have also paid attention to the solid-state perovskite solar cells with energy conversion efficiency exceeding 10%, in which mesoporous TiO_2 functions as an electron transport layer.[178, 179] The appearing prospects of TiO_2 NT application in betavoltaics are discussed below.

The TiO_2 NT-based structures are used to produce betavoltaic batteries with a long service life, which efficiently convert the energy of β-radiation to electricity.[180 – 184] High energy conversion characteristics of these devices are provided by several factors. The first one is selection of electrode materials for the generation of an internal field between the metal electrodes and Schottky barriers at the metal/semiconductor interfaces. The second factor is that an array of TiO_2 NTs has a larger specific surface area, enhanced characteristics of the electron trans-

Table 1. Parameters of memristor structures based on TiO_2 active layer.

Memristor	Thickness of the active layer, nm	Method of synthesis	Morphology	Type of structure	Type of filaments	R_{HRS}/R_{LRS}	Ref.
Pt/TiO_2/Pt	60	Atomic-layer deposition	Film	Anatase, brookite	V_O	4 – 20	161, 162
Pt/TiO_2/Ti	< 100	Anodization	Film	–	V_O	–	150
Au/TiO_2/FTO [a]	–	Electrochemical deposition	Nanotubes	Anatase	V_O	~ 10	153
Pt/TiO_2/Ti	~ 200	Anodization	Nanotubes	Amorphous	V_O	14	154
Cu/TiO_2/Ti	3000	Anodization	Nanotubes	Anatase	V_O	–	155
Ti/TiO_2/Au	500	Anodization	Nanotubes	–	V_O	60	156
Pt/TiO_2/Ti	~ 100	Anodization	Film	Amorphous	V_O	~ 12	163
Ti/TiO_2/Pt	250	Anodization	Nanotubes	Amorphous (initial), anatase (after annealing)	V_O	1 – 5	157
Cu/TiO_2/Ti	8 – 29	Anodization	Film	–	–	< 80	151
Au/TiO_2/Pt	~ 100	Atomic-layer deposition	Film	Amorphous	V_O	~ 100	164
Ti/TiO_2/Au	120 – 200	Anodization	Nanotubes	Amorphous	V_O	130 – 440	158
Ag/TiO_2/Ti	750 – 2300	Anodization	Film	Amorphous	Ag	~ 27	152
Au/Cu/TiO_2/Ti	~ 5000	Anodization	Nanotubes	Amorphous (initial), anatase (after annealing)	Cu	> 20	159
Au/TiO_2/Ti	1800 – 2100	Anodization	Nanotubes	Anatase (after annealing)	V_O	19	160

[a] FTO is fluorine-doped tin oxide (fluorine-doped SnO_2 film).

fer along the nanotubes, more efficient absorption of β-particles and a higher radiation stability than planar structures.

The determination procedures and calculation equations for the key characteristics of betavoltaic cells, *i.e.*, open-circuit voltage (U_{oc}), short-circuit current (I_{sc}), the maximum specific power output (P_{max}), the fill factor (FF) and the energy conversion efficiency (η), are comprehensively described in the literature.[180–189] By analogy with planar structures, the parameters of betavoltaic cells were normalized to the geometric area of the active layer with TiO_2 nanotubes.[185–189]

Zhang *et al.*[180] studied the betavoltaic effect in the Ni/^{63}Ni/NT TiO_2/Ti sandwich structure. The TiO_2 NT layer was synthesized in an ethylene glycol-based electrolyte containing 3.0 vol.% H_2O and 0.5 mass % NH_4F at a constant voltage of 60 V for 2–8 h followed by annealing under nitrogen at 450–500 °C for 4 h. When the activity of the ^{63}Ni source was 10 mCi, the following characteristics were obtained for a cell with a geometric area of 2.4 cm^2 fabricated from 11 μm-long tubes of 130 nm diameter: U_{oc} = 1.54 V, I_{sc} = 12.43 nA, P_{max} = 2.98 nW cm^{-2}, FF = 0.47 and η = 1.11%. In the general case, the diameter and length of TiO_2 NTs affect the conversion efficiency.

An important role of the V_O and Ti^{3+} centres in the improvement of characteristics of betavoltaic cells based on modified layers of TiO_2 nanotubes was noted.[181,182] For example, cells based on an TiO_2 NT layer annealed in an argon atmosphere at 650 °C showed the following characteristics:[182] η = 3.65% for U_{oc} = 1.13 V, I_{sc} = 103.3 nA cm^{-2} and FF = 0.32. The maximum power output for these cells was 37 nW cm^{-2}, which is twice as high as that for the cells based on TiO_2 NT layers annealed in air. In addition, P_{max} increased by 30% as the annealing temperature was raised from 450 to 650 °C, which was attributed to the formation of a rutile phase.

Ma *et al.*[181] reported betavoltaic cells based on TiO_2 NT layers that were annealed at 450 °C and electrochemically reduced *via* cathodic treatment at 50 V voltage in ethylene glycol for 35 s. The cells had the following characteristics: η = 3.79% for U_{oc} = 1.04 V, I_{sc} = 117.5 nA cm^{-2}, FF = 0.32 and P_{max} = 39.2 nW cm^{-2}.

Considerable attention is also devoted to improving the electrical contact between the Ni electrode and the array of nanotubes. For example, the electrodeposition of graphene oxide (GO) on TiO_2 NTs markedly increases the energy conversion efficiency. The following characteristics were found[183] for the Ni/^{63}Ni/GO/NT TiO_2/Ti betavoltaic cell with an area of 2 cm^2 and a ^{63}Ni source activity of 10 mCi: η = 3.93% for U_{oc} = 2.38 V, I_{sc} = 27.2 nA and FF = 0.58. The maximum specific power output of this cell was 37.4 nW cm^{-2}, which is commensurable with this value for betavoltaic cells based on modified TiO_2 NT layers.[181,182]

Using the data presented in Table 2, it is possible to compare the active layer morphology and the key parameters of betavoltaic cells based on functional layers of TiO_2 NTs with analogous characteristics of betavoltaic cells with planar diode structures made of different materials [Si,[185] 4*H*-SiC,[186] GaN (Ref. 187) and C (diamond)[188]]. It can be seen that the outer diameter and wall thickness of nanotubes in the active layer are virtually equal, amounting to 100–130 and 10–20 nm, respectively. The active layer thickness optimal for a betavoltaic cell is ~10 μm. It is noteworthy that cell characteristics are also affected by modification of the initial TiO_2 NT layers, which brings about an increase in η from 1.11 to 3.65–3.93% and an increase in P_{max} by an order of magnitude, from ~3 to > 30 nW cm^{-2}. The latter value is several times higher than P_{max} for the betavoltaic cell with a planar diode structure.[189] In addition, when self-absorption of β-radiation, resulting in decreasing effective activity of the source is taken into account, the estimated η increases to 7.3 (Ref. 180) and 26.55%.[183,184] This indicates good prospects for the design of high-performance betavoltaic cells based on functional layers of TiO_2 NTs.

4.4. Supercapacitors

Owing to the high specific surface area and chemical stability, TiO_2 NTs are promising as a material for the fabrication of supercapacitors with an electrical double layer.[190–192] The vertically arranged and spatially ordered nanotubes on a titanium substrate provide better characteristics of the electron transport along the nanotubes than chaotically arranged nanostructures; furthermore, the substrate can be directly used as a supercapacitor electrode. The nanotubes open on one end are also suitable for the fabrication of composite nanomaterials without the use of binding agents. Nevertheless, owing to low electrical con-

Table 2. Structures and characteristics of known betavoltaic cells.

Structure	Thickness of the active layer, μm	Outer diameter, nm	Wall thickness, nm	Method of synthesis	Modification	P_{max}, nW cm^{-2}	η (%)	Ref.
Ni/^{63}Ni/TiO_2/Ti	11	130	20	Anodization	Annealing in N_2	2.98	1.11	180
	10	100	10	Anodization	Cathodic treatment	39.2	3.79	181
Ni/^{63}Ni/GO/TiO_2/Ti	8	100	10	Anodization	Annealing in Ar	37	3.65	182
	4	130	10	Anodization	Annealing in N_2, electrodeposition	37.4	3.93	183, 184
4*H*-SiC (p–n-diode)	4 (p-layer), 0.25 (n-layer)	–	–	Chemical vapour deposition	–	6.16	6	186
GaN (p–i–n-diode)	1.0 (n-layer), 0.9 (i-layer), 0.05 (p-layer)	–	–	Chemical vapour deposition	–	12.25	0.98	187
C(diamond)/Pt (Schottky diode)	50 (p-layer), 0.025 (Pt-layer)	–	–	Chemical vapour deposition	Magnetron sputtering	3	0.6	188
Si (p–i–n-diode)	470 (all layers)	–	–	Ion implantation	–	6.14	0.6	185
					Annealing in N_2	3.53	0.35	185

ductivity, electrodes based on the initial amorphous TiO_2 NTs have a relatively low specific surface capacitance $C_s = 10-40$ μF cm^{-2} in non-faradaic charge–discharge processes.[193, 194] In order to increase the specific surface capacitance, TiO_2 nanotubes with variable geometry are synthesized and are modified in different ways.

The anodization conditions are often varied and the heat treatment is carried out in air.[192, 193, 195] For example, it was shown [195] that TiO_2 NTs synthesized in electrolytes based on glycerol, ethylene glycol and deionized water in 70 : 30 : 2 and 50 : 50 : 2 volume ratios containing 0.3 M ammonium fluoride at a constant voltage of 50 V for four hours and subsequently annealed at 450 °C for three hours had a maximum specific capacitance of 1300 μF cm^{-2} at a rate of voltage change $\Delta U = 20$ mV s^{-1}.

The authors of many studies modified TiO_2 NTs by heat treatment under argon,[192, 196] argon and air mixture,[192] hydrogen [194, 197, 198] and ammonia.[199–202] Zhou and Zhang [192] obtained $C_s = 911$ μF cm^{-2} at $\Delta U = 1$ mV s^{-1} for TiO_2 NTs synthesized in an electrolyte based on glycerol and deionized water in 9 : 1 volume ratio containing 0.3 mass % NH_4F at a constant voltage of 15 V for 17 h followed by annealing in an argon atmosphere at 630 °C for an hour.

Salari *et al.*[193] found the values $C_s = 3240$ μF cm^{-2} at $\Delta U = 100$ mV s^{-1} for TiO_2 NTs synthesized in an electrolyte based on glycerol and deionized water in 9 : 1 molar ratio containing 0.75% NH_4F at a constant voltage of 30 V for three hours and subsequently annealed under argon for an hour at 400 °C. It was noted [192, 193] that the heat treatment of TiO_2 NTs in air causes an insignificant improvement of the capacitance characteristics.

Xie *et al.*[201] showed that the heat treatment of TiO_2 NTs in an atmosphere of ammonia (nitriding) at 800 °C for three hours gives rise to a nanotubular TiN structure and markedly increases the specific conductivity up to

Table 3. Characteristics of supercapacitor electrodes based on an TiO_2 NT layer.

Electrode	Thickness of the active layer, μm	Outer diameter, nm	NT wall thickness, nm	Modification	Structure	C_s, mF cm^{-2}	Ref.
TiO_2	0.9–1.0	30–60	10–20	None	Amorphous	0.01–0.04	193
	1.2	100	20	None	Amorphous	0.01–0.04	194
	1.2	100	20	Annealing in air	Anatase	0.08	194
	0.80–0.95	130–160	10–20	Annealing in air	Anatase	0.45	219
	0.9–1.0	130–165	10–15	Annealing in air	Anatase	0.26	201
	10.5–10.7	90–110	10	Annealing in air	Anatase	7.8	201
	2.8	100	–	Annealing in air	Anatase	1.12	203
	0.9–1.0	30–60	10–20	Annealing in air	Anatase, rutile	0.03	193
				Annealing in air with Ar	Anatase, rutile	0.294	193
				Annealing in Ar	Anatase, rutile	0.911	193
	1.2	100	20	Annealing in H_2	Anatase	3.24	194
	0.9–1.0	130–165	10–15	Annealing in NH_3	Cubic TiN	3.14	201
	10.5–10.7	90–110	10	Annealing in NH_3	Cubic TiN	83.6	201
	0.9–1.0	130–165	10–15	Annealing in air, cathodic treatment	Anatase	3.14	201
	14.5	115–140	–	Annealing in air, hydrogen plasma treatment	Anatase	7.22	208
TiO_2 : Fe	0.176	30	–	Anodization with the addition of $Fe(NO_3)_3$, annealing in air	Anatase	1.11	205
TiO_2 : Mn	3.5	110	10	Anodization of the Ti–Mn alloy, annealing in air	Anatase	1.6	204
TiO_2 : Al	2.8	85	–	Annealing in air, cathodic treatment	Anatase	1.8–3.5	203
TiO_2 (see [a])	–	100	–	Deposition	–	4.4	215
TiO_2 : Al–MnO_2	3.1–6.4	150–200	–	Annealing in air, cathodic treatment, electrodeposition	Anatase	17	203
TiO_2–PPy [b]	0.80–0.95	130–160	10–20	Annealing in air, pulsed electrodeposition	Anatase	33.1	219
TiO_2–C	2–4	90	–	Vacuum infiltration, annealing in air	Amorphous	40.75	216
TiO_2–MnO_2	5.4	150–200	10–20	Annealing in air, cathodic treatment, electrodeposition	Anatase	150.9	203
TiO_2–C–MnO_2	~1 [c]	115–125	15–25	Gas thermal adsorption, electrodeposition	Anatase, rutile	492	214

[a] Multi-walled carbon nanotubes; [b] PPy is polypyrrole (conducting polymer); [c] estimated by the authors of this review using data of Ref. 214.

4.5×10^6 S m^{-1}. This fact is responsible for increasing specific capacitance of the electrode from 260 to 3140 μF cm^{-2} for $\Delta U = 20$ mV s^{-1} (according to cyclic voltammetry data).

In some studies, TiO_2 NTs were modified by electrochemical method, particularly, they were doped with metals such as aluminium,[203] manganese [204] and iron,[205] and also using self-doping during cathodic treatment (hydrogenation).[191, 206, 207] For example, Zhong *et al.*[203] described the following procedure of doping of the initial TiO_2 NTs with aluminium ions. First, TiO_2 NT samples were synthesized in an electrolyte based on ethylene glycol and deionized water taken in 24 : 1 volume ratio containing 0.3 mass % NH_4F at a constant voltage of 60 V, with the secondary anodization time being 20 min. The samples thus formed were annealed in air at 450 °C for two hours. Then cathodic treatment of TiO_2 NTs was carried out in a 1 M $AlCl_3$ solution in the galvanostatic mode at a current of 0.2 mA cm^{-2} for 25–250 s. This modification was accompanied by insertion of not only Al^{3+} ions, but also H^+ ions into TiO_2 NTs. During this process, Ti^{4+} was reduced to Ti^{3+}, which gave rise to additional oxygen vacancies and thus improved the conductivity. This, in turn, resulted in an increase in C_s to 3510 and 2740 μF cm^{-2} at $\Delta U = 10$ and 100 mV s^{-1}, respectively.

In the case of hydrogenated (self-doped) TiO_2 NT samples, $C_s = 1840$ μF cm^{-2} at $\Delta U = 5$ mV s^{-1} (Ref. 191). Zhang *et al.*[205] carried out the cathodic treatment in an aqueous solution of Na_2SO_4 at a -1.5 V voltage of TiO_2 NT electrodes synthesized in an ethylene glycol-based electrolyte containing 2 mass % H_2O and 0.3 mass % NH_4F at a constant voltage of 50 V for four hours followed by annealing in air at 450 °C for two hours. These electrodes showed high stability in $> 2 \times 10^3$ cycles at $\Delta U = 100$ mV s^{-1} and record-high values $C_s = 11.37$ mF cm^{-2} for $\Delta U = 100$ mV s^{-1} and $C_s = 12.0$ mF cm^{-2} for a current density of 1 mA cm^{-2}.

Hydrogen plasma treatment of the initial TiO_2 NT samples also enhances the capacitance characteristics of electrodes due to the formation of Ti^{3+} centres and insertion of OH groups.[208, 209] In particular, Wu *et al.*[208] synthesized TiO_2 NTs in an ethylene glycol-based electrolyte containing 2 vol.% H_2O and 0.5 mass % NH_4F at a constant voltage of 60 V for two hours followed by annealing in air at 450 °C for three hours; the nanoparticles were modified in a hydrogen plasma. These electrodes showed the following maximum values: $C_s = 7.22$ and 6.37 mF cm^{-2} for the current density of 0.5 and 2.0 mA cm^{-2}, respectively, in charge–discharge processes and also demonstrated high stability over $> 10^4$ cycles at a current density of 0.1 mA cm^{-2}.

Efficient composite electrodes are also fabricated by modification of TiO_2 NTs with metal oxide nanoparticles,[199, 210–214] carbon nanomaterials [212, 214–218] and conducting polymers,[219–223] which substantially improves their capacitance characteristics. For example, TiO_2 NT samples subjected to cathodic treatment in a 0.5 M aqueous solution of Na_2SO_4 at -1.4 V (self-doping) for 10 min at 25 °C and then decorated with MnO_2 particles along the whole nanotube length showed C_s of 150.9 mF cm^{-2}, which is the highest value among the MnO_2-TiO_2 composites.[210]

The geometric parameters and specific surface capacitances for the initial, modified and composite electrodes based on TiO_2 NT layers are summarized in Table 3. It can be seen that TiO_2 electrodes are 0.2 to 10 μm thick and consist of nanotubes with an outer diameter ranging from 30 to 200 nm and wall thickness ranging from 10 to 25 nm. The C_s values increase with increasing thickness of the active layer and with decreasing diameter of nanotubes. Analysis of the data of Table 3 indicates that for attaining the highest C_s values, it is preferable to use simultaneously several methods for modification of the initial TiO_2 NT arrays. In the first stage, one of the following procedures is employed: annealing in air or in an inert atmosphere followed by hydrogen plasma treatment or cathodic treatment, annealing under H_2 or NH_3. In the second stage, the resulting samples are modified by conducting polymers, carbon nanomaterials and/or oxide nanoparticles. The highest value $C_s = 492$ mF cm^{-2} for a specific surface energy of 465 mW h m^{-2} was obtained for the $TiO_2-C-MnO_2$ composite electrodes.[214]

5. Note added in proof

When the review was being prepared for publication, the papers that appeared in scientific journals of various disciplines were mainly devoted to the application of materials based on nanotubular titanium dioxide (see Section 4 of this review). In particular, mention should be made of publications summarizing the use of 1D anodized titanium structures for the manufacture of biocompatible implants [224–226] and for other medical applications,[227] as high-performance gas sensors,[228] and for solving applied problems of green chemistry.[229–231] Several new reviews address the prospects of using TiO_2 nanotubes in modern alternative energy devices [232–234] and new designed high-performance solar batteries.[235–237] Section 4.2 'Nanoelectronics, memristors' of this review considering devices for the next-generation resistive memory can be supplemented by the study [238] addressing the memristive properties of hybrid nanostructures based on a nanotubular anatase layer and rutile nanorods with inclusions of Pt and/or Pd–Pt nanoparticles. The authors observed stable reproducible bipolar switching for > 100 cycles, enhanced stability of the resistive states and slightly increased on to off current ratio of the designed memristor.

6. Conclusion

Nanotubular titanium dioxide is an environmentally safe (non-toxic), economically available and efficient functional material, which is extensively used. Stoichiometric and non-stoichiometric TiO_2 nanotubes are attracting ever increasing attention of researchers all over the world, since they can be applied as photocatalysts for the synthesis of organic molecules in high yields in conformity with the green chemistry principles. It is expected that the non-stoichiometric modified titanium dioxide, which, unlike stoichiometric TiO_2, absorbs visible light will be mainly used as a photocatalyst, with photocatalytic activity being attained without illumination with a harmful and expensive UV light.

An efficient approach for conversion of stoichiometric TiO_2 to the nonstoichiometric form is to generate point defects, particularly, oxygen vacancies, which results in a change in the atomic structure and optical and electronic properties of the material. The change in the electronic structure under the action of visible light leads to enhanced photocatalytic activity in the synthesis of organic compounds, which are in-demand in medicinal

chemistry for the green synthesis of pharmaceutical agents.

Memristor structures are usually fabricated using high-tech and expensive molecular beam epitaxy and chemical vapour deposition methods. In this connection, it appears promising to develop a nanotechnology for combining, at the atomic level, ideal and oxygen nonstoichiometric layers of a semiconductor or dielectric between metal electrodes. It is demonstrated in the review that memristive behaviour in nanostructures of nonstoichiometric titanium dioxide is provided, as a rule, by the mobility of cationic and anionic vacancies in the dielectric layer, while its thickness and defectiveness determine the electrical resistance of the structure in the low- and high-resistance and intermediate states. The possibility of formation and control of conductive states over a wide range of charge carrier mobility for memristor structures based on nanotubular TiO_2 arrays allows the use of these structures as solid-state physical models of synapses with high plasticity. This, in turn, opens up new prospects for the fabrication of efficient functional media for solid-state implementation of neural computing systems and artificial neural networks.

This review was prepared with financial support of the Russian Foundation for Basic Research (Projects No. 19-13-50254-ekspansiya and No. 20-03-00299) and the Ministry of Science and Higher Education of the Russian Federation (Project FEUZ-2020-0059).

7. List of acronyms and designations

TEM — transmission electron microscopy,
XPS — X-ray photoelectron spectroscopy,
HRS — high resistance state,
LRS — low resistance state,
GO — graphene oxide,
NT — nanotube,
PAA — polyacrylic acid,
C_s — specific surface capacitance,
FF — fill factor,
I_{sc} — short-circuit current,
N — number of full cycles of resistive switching of the memristor,
P_{max} — maximum specific power output,
R_{HRS} — electrical resistance of the memristor in the high-resistance state,
R_{LRS} — electrical resistance of the memristor in the low-resistance state,
U_{oc} — open-circuit voltage,
ΔU — rate of voltage change,
η — energy conversion efficiency.

References

1. M.Ge, C.Cao, J.Huang, L.S.Shuhui, Z.Chen, K.Q.Zhang, S.S.Al-Deyab, L.Y.J.Yuekun. *Mater. Chem. A*, **4**, 6772 (2016)
2. V.Augugliaro, T.Caronna, A.Paola, G.Marcì, M.Pagliaro, G.Palmisano, L.Palmisano. In *Environmentally Benign Photocatalysts*. (Eds M.Anpo, P.V.Kamat). (New York: Springer, 2010). P. 623
3. A.A.Valeeva, A.A.Rempel, S.V.Rempel, S.I.Sadovnikov, A.I.Gusev. *Russ. Chem. Rev.*, **90**, 601 (2021)
4. I.B.Dorosheva, A.A.Valeeva, A.A.Rempel, M.A.Trestsova, I.A.Utepova. *Inorg. Mater.*, **57**, 503 (2021)
5. A.A.Sushnikova, A.A.Valeeva, I.B.Dorosheva, A.A.Rempel. *Fiz. Tv. Tela*, **63**, 2016 (2021); https://doi.org/10.21883/FTT.2021.12.51659.172s
6. A.K.Vasilevskaia, V.I.Popkov, A.A.Valeeva, A.A.Rempel. *Russ. J. Appl. Chem.*, **89**, 1211 (2016)
7. I.B.Dorosheva, A.A.Valeeva, A.A.Rempel. *AIP Conference Proceedings*, **1886**, 020006 (2017); https://doi.org10.1063/1.5002903
8. V.I.Popkov, A.K.Bachina, A.A.Lobinsky, E.Y.Gerasimov, A.A.Valeeva, A.A.Rempel. *Ceram. Int.*, **46**, 24483 (2020)
9. I.B.Dorosheva, A.A.Rempel, A.A.Valeeva, I.A.Weinstein. *KnE Soc. Sci.*, **6**, 1 (2020)
10. A.A.Valeeva, I.B.Dorosheva, I.A.Weinstein, A.A.Rempel, E.A.Kozlova. *KnE Soc. Sci.*, **6**, 19 (2020)
11. A.A.Valeeva, I.B.Dorosheva, E.A.Kozlova, A.A.Sushnikova, A.Y.Kurenkova, A.A.Saraev, H.Schroettner, A.A.Rempel. *Int. J. Hydrogen Energy*, **46**, 16917 (2021)
12. P.Roy, S.Berger, P.Schmuki. *Angew. Chem., Int. Ed.*, **50**, 2904 (2011)
13. I.Paramasivam, H.Jha, N.Liu, P.Schmuki. *Small*, **8**, 3073 (2012)
14. P.Roy, D.Kim, K.Lee, E.Spiecker, P.Schmuki. *Nanoscale*, **2**, 45 (2010)
15. Q.Zhang, G.Cao. *Nano Today*, **6**, 91 (2011)
16. Y.Li, X.Yu, Q.Yang. *J. Sens.*, **2009**, 19 (2009)
17. T.Ochiai, A.Fujishima. *J. Photochem. Photobiol. C*, **13**, 247 (2012)
18. S.Maher, J.Qin, K.Gulati, A.ElMekawy, G.Kaur, L.Lima-Marques, G.Atkins, D.M.Findlay, A.Evdokiou, D.Losic. *3D Printed Titanium Implants with Nanoengineered Surface Titania Nanotubes for Localized Drug Delivery (Conference Paper)*. (Australia: Engineers Australia, Barton, A.C.T., 2016). P. 65
19. Y.Y.Khrunyk, I.V.Vyalykh, A.V.Korelin, S.V.Belikov, M.S.Karabanalov, S.B.Rakitin, R.V.Kamalov, A.A.Popov. *Dokl. Biol. Sci.*, **475**, 175 (2017)
20. K.von Der Mark, J.Park, S.Bauer, P.Schmuki. *Cell Tissue Res.*, **339**, 131 (2009)
21. A.Fujishima, K.Honda. *Nature (London)*, **238**, 37 (1972)
22. A.Fujishima, T.N.Rao, D.A.Tryk. *J. Photochem. Photobiol. C*, **1**, 1 (2000)
23. D.A.Tryk, A.Fujishima, K.Honda. *Electrochim. Acta*, **45**, 2363 (2000)
24. X.Li, L.Wang, Y.Fan, Q.Feng, F.Cui. *J. Nanomater.*, 6 (2012)
25. E.A.Goodilin, P.S.Weiss, Yu.Gogotsi. *ACS Nano*, **13**, 10879 (2019)
26. D.I.Petukhov, A.A.Eliseev, I.V.Kolesnik, K.S.Napolskii, A.V.Lukashin, A.V.Garshev, Y.D.Tretyakov, D.Chernyshov, W.Bras, S.-F.Chen, C.-P.Liu. *J. Porous Mater.*, **19**, 71 (2012)
27. I.A.Utepova, M.A.Trestsova, O.N.Chupakhin, V.N.Charushin, A.A.Rempel. *Green Chem.*, **17**, 4401 (2015)
28. E.A.Kozlova, N.S.Kozhevnikova, S.V.Cherepanova, T.P.Lyubina, E.Yu.Gerasimov, V.V.Kaichev, A.V.Vorontsov, S.V.Tsybulya, A.A.Rempel, V.N.Parmon. *J. Photochem. Photobiol. A*, **250**, 10 (2012)
29. V.P.Ananikov, L.L.Khemchyan, Y.V.Ivanova, V.I.Bukhtiyarov, A.M.Sorokin, I.P.Prosvirin, S.Z.Vatsadze, A.V.Medved'ko, V.N.Nuriev, A.D.Dilman, V.V.Levin, I.V.Koptyug, K.V.Kovtunov, V.V.Zhivonitko, V.A.Likholobov, A.V.Romanenko, P.A.Simonov, V.G.Nenajdenko, O.I.Shmatova, V.M.Muzalevskiy, M.S.Nechaev, A.F.Asachenko, O.S.Morozov, P.B.Dzhevakov, S.N.Osipov, D.V.Vorobyeva, M.A.Topchiy, M.A.Zotova, S.A.Ponomarenko, O.V.Borshchev, Y.N.Luponosov, A.A.Rempel, A.A.Valeeva, A.Y.Stakheev, O.V.Turova, I.S.Mashkovsky, S.V.Sysolyatin, V.V.Malykhin, G.A.Bukhtiyarova, A.O.Terent'ev, I.B.Krylov. *Russ. Chem. Rev.*, **83**, 885 (2014)

30. I.A.Utepova, O.N.Chupakhin, M.A.Trestsova, A.A.Musikhina, D.A.Kucheryavaya, V.N.Charushin, A.A.Rempel, N.S.Kozhevnikova, A.A.Valeeva, A.I.Mikhaleva, B.A.Trofimov. *Russ. Chem. Bull., Int. Ed.*, **65**, 445 (2016)
31. A.A.Rempel, E.A.Kozlova, T.I.Gorbunova, S.V.Cherepanova, E.Yu.Gerasimov, N.S.Kozhevnikova, A.A.Valeeva, E.Yu.Korovin, V.V.Kaichev, Yu.A.Shchipunov. *Catal. Commun.*, **68**, 61 (2015)
32. I.B.Dorosheva, A.A.Rempel, M.A.Trestsova, I.A.Utepova, O.N.Chupakhin. *Inorg. Mater.*, **55**, 155 (2019)
33. S.Higashimoto, N.Suetsugu, M.Azuma, H.Ohue, Y.Sakata. *J. Catal.*, **27**6, 76 (2010)
34. A.A.Valeeva, E.A.Kozlova, A.S.Vokhmintsev, R.V.Kamalov, I.B.Dorosheva, A.A.Saraev, I.A.Weinstein, A.A.Rempel. *Sci. Rep.*, **8**, 9607 (2018)
35. A.A.Valeeva, I.B.Dorosheva, E.A.Kozlova, R.V.Kamalov, A.S.Vokhmintsev, D.S.Selishchev, A.A.Saraev, E.Yu.Gerasimov, I.A.Weinstein, A.A.Rempel. *J. Alloys Compd.*, **796**, 293 (2019)
36. V.M.Zainullina, V.P.Zhukov, M.A.Korotin. *J. Photochem. Photobiol. C*, **22**, 58 (2015)
37. I.B.Dorosheva, E.V.Adiyak, A.A.Valeeva, A.A.Rempel. *AIP Conference Proceedings*, **2174**, 020019 (2019); https://doi.org/10.1063/1.5134170
38. A.A.Rempel, A.A.Valeeva. *Russ. Chem. Bull., Int. Ed.*, **68**, 2163 (2019)
39. A.A.Rempel, Y.V.Kuznetsova, I.B.Dorosheva, A.A.Valeeva, I.A.Weinstein, E.A.Kozlova, A.A.Saraev, D.S.Selishchev. *Top. Catal.*, **63**, 130 (2020)
40. S.Iijima. *Nature (London)*, **354**, 56 (1991)
41. S.Iijima, T.Ichihashi. *Nature (London)*, **363**, 603 (1993)
42. R.Tenne, L.Margulis, M.Genut, G.Hodes. *Nature (London)*, **360**, 444 (1992)
43. Yu.D.Tretyakov, E.A.Goodilin. *Russ. Chem. Rev.*, **78**, 801 (2009)
44. A.Yu.Polyakov, A.Zak, R.Tenne, E.A.Goodilin, K.A.Solntsev. *Russ. Chem. Rev.*, **87**, 251 (2018)
45. L.Pauling. *Proc. Natl. Acad. Sci. USA*, **16**, 578 (1930)
46. T.F.Bates, L.B.Sand, J.F.Mink. *Science*, **111**, 512 (1950)
47. S.V.Krivovichev. In *Minerals as Advanced Materials. I.* (Ed. S.Krivovichev). (Berlin, Heidelberg: Springer-Verlag, 2008). P. 179
48. S.A.Chivilikhin, I.Yu.Popov, V.V.Gusarov. *Dokl. Phys.*, **52**, 60 (2007)
49. A.A.Krasilin, E.K.Khrapova, A.Nomine, J.Ghanbaja, T.Belmonte, V.V.Gusarov. *ChemPhysChem.*, **20**, 719 (2019)
50. M.Assefpour-Dezfuly, C.Vlachos, E.H.Andrews. *J. Mater. Sci.*, **19**, 3626 (1984)
51. V.Zwilling, M.Aucouturier, E.Darque-Ceretti. *Electrochim. Acta*, **45**, 921 (1999)
52. K.Lee, A.Mazare, P.Schmuki. *Chem. Rev.*, **114**, 9385 (2014)
53. Y.Fu, A.Mo. *Nanoscale Res. Lett.*, **13**, 187 (2018)
54. L.X.Yang, S.L.Luo, Q.Y.Cai, S.Z.Yao. *Chin. Sci. Bull.*, **55**, 331 (2010)
55. H.-H.Ou, S.-L.Lo. *Sep. Purif. Technol.*, **58**, 179 (2007)
56. X.Chen, S.S.Mao. *Chem. Rev.*, **107**, 2891 (2007)
57. T.Kasuga, M.Hiramatsu, A.Hoson, T.Sekino, K.Niihara. *Adv. Mater.*, **11**, 1307 (1999)
58. J.Yang, S.Mei, J.M.F.Ferreira. *Mater. Sci. Eng. C*, **15**, 183 (2001)
59. S.Y.Chae, M.K.Park, S.K.Lee, T.Y.Kim, S.K.Kim, W.I.Lee. *Chem. Mater.*, **15**, 3326 (2003)
60. B.B.Lakshmi, P.K.Dorhout, C.R.Martin. *Chem. Mater.*, **9**, 857 (1997)
61. J.H.Jung, H.Kobayashi, K.J.C.van Bommel, S.Shinkai, T.Shimizu. *Chem. Mater.*, **14**, 1445 (2002)
62. D.Losic, M.S.Aw, A.Santos, K.Gulati, M.Bariana. *Exp. Opin. Drug Deliv.*, **12**, 103 (2015)
63. M.Macák. Dis. Dipl.- Ing.Universität Erlangen-Nürnberg, Erlangen, 2008
64. M.Lee, T.Kim, C.Bae, H.Shin, J.Kim. *JOM*, **62**, 44 (2010)
65. P.Hoyer. *Langmuir*, **12**, 1411 (1996)
66. H.Shin, D.-K.Jeong, J.Lee, M.M.Sung, J.Kim. *Adv. Mater.*, **16**, 1197 (2004)
67. T.Kasuga, M.Hiramatsu, A.Hoson, T.Sekino, K.Niihara. *Langmuir*, **14**, 3160 (1998)
68. O.B.Kotova *Vestn. In-ta Geolog. Komi NC Ural RAN*, **10**, 8 (2007)
69. G.H.Du, Q.Chen, R.C.Che, Z.Y.Yuan, L.-M.Peng. *Appl. Phys. Lett.*, **79**, 3702 (2001)
70. X.Sun, Y.Li. *Chem. – Eur. J.*, **9**, 2229 (2003)
71. X.Wu, Q.-Z.Jiang, Z.-F.Ma, M.Fu, W.-F.Shangguan. *Solid State Commun.*, **136**, 513 (2005)
72. I.S.Bodalyov, A.A.Malkov, E.N.Korytkova, T.P.Maslennikova, A.A.Malygin. *Russ. J. Appl. Chem.*, **87**, 151 (2014)
73. A.A.Krasilin, I.S.Bodalyov, A.A.Malkov, E.K.Khrapova, T.P.Maslennikova, A.A.Malygin. *Nanosystems: Phys., Chem., Mathem.*, **9**, 410 (2018)
74. M.S.Sander. M.J.Côté, W.Gu, B.M.Kile, C.P.Tripp. *Adv. Mater.*, **16**, 2052 (2004)
75. Y.Lin, G.S.Wu, X.Y.Yuan, T.Xie, L.D.Zhang. *J. Phys.: Condens. Matter*, **15**, 2917 (2003)
76. T.P.Maslennikova, O.Yu.Sinel'shchikova, N.V.Besprozvannykh, E.N.Gatina, S.K.Kuchaeva, V.L.Ugolkov. *Russ. J. Appl. Chem.*, **90**, 193 (2017)
77. J.J.Kelly. *Electrochim. Acta*, **24**, 1273 (1979)
78. A.B.Denisenko, A.N.Morozov, A.I.Mikhailichenko. *Usp. Khim. Khim. Tekhnol.*, **29** (3), 71 (2015)
79. V.Zwilling, E.Darque-Ceretti, A.Boutry-Forveille, D.David, M.Y.Perrin, M.Aucouturier. *Surface Interface Anal.*, **27**, 629 (1999)
80. J.M.Macak, K.Sirotna, P.Schmuki. *Electrochim. Acta*, **50**, 3679 (2005)
81. M.Paulose, H.E.Prakasam, O.K.Varghese, L.Peng, K.C.Popat, G.K.Mor, T.A. Desai, C.A.Grimes. *J. Phys. Chem. C*, **111**, 14992 (2007)
82. D.A.Buldakov, D.I.Petukhov, I.V.Kolesnik, A.A.Eliseev, A.V.Lukashin, Yu.D.Tret'yakov. *Nanotechnol. Russ.*, **4**, 296 (2009)
83. D.Gong, C.Grimes, O.Varghese. *J. Mater. Res.*, **16**, 331 (2001)
84. R.Hahn, J.M.Macak, P.Schmuki. *Electrochem. Commun.*, **9**, 947 (2007)
85. M.D.Ye, J.J.Gong, Y.K.Lai, C.J.Lin, Z.Q.Lin. *J. Am. Chem. Soc.*, **134**, 15720 (2012)
86. M.Z.Ge, S.H.Li, J.Y.Huang, K.Q.Zhang, S.S.Al-Deyab, Y.K.Lai. *J. Mater. Chem. A*, **3**, 3491 (2015)
87. Y.Lai, H.Zhuang, L.Sun, Z.Chen, C.Lin. *Electrochim. Acta*, **54**, 6536 (2009)
88. J.Wang, Z.Lin. *J. Phys. Chem. C*, **113**, 4026 (2009)
89. Q.Y.Cai, M.Paulose, O.K.Varghese, C.A.Grimes. *J. Mater. Res.*, **20**, 230 (2005)
90. D.Wang, Y.Liu, B.Yu, F.Zhou, W.Liu. *Chem. Mater.*, **21**, 1198 (2009)
91. K.S.Raja, T.Gandhi, M.Misra. *Electrochem. Commun.*, **9**, 1069 (2007)
92. V.M.Pridaa, E.Manova, V.Vega, M.Hernandez-Velez, P.Aranda, K.R.Pirota, M.Vazquez, E.Ruiz-Hitzky. *J. Magn. Magn. Mater.*, **316**, 110 (2007)
93. J.Wang, Z.Lin. *Chem. Mater.*, **20**, 1257 (2008)
94. X.Meng, T.Y.Lee, H.Chen, D.W.Shin, K.W.Kwon, S.J.Kwon, J.B.Yoo. *J. Nanosci. Nanotechnol.*, **10**, 4259 (2010)
95. D.A.Wang, L.F.Liu. *Chem. Mater.*, **22**, 6656 (2010)
96. J.M.Macak, H.Tsuchiya, L.Taveira, S.Aldabergerova, P.Schmuki. *Angew. Chem., Int. Ed.*, **44**, 7463 (2005)
97. C.Ruan, M.Paulose, O.K.Varghese, G.K.Mor, C.A.Grimes. *J. Phys. Chem. B*, **109**, 15754 (2005)

98. N.K.Allam, C.A.Grimes. *J. Phys. Chem. B*, **111**, 13028 (2007)
99. R.Beranek, H.Hildebrand, P.Schmuki. *Electrochem. Solid-State Lett.*, **6**, B12 (2003)
100. S.P.Albu, A.Ghicov, S.Aldabergenova, P.Drechsel, D.LeClere, G.E.Thompson, J.M.Macak, P.Schmuki. *Adv. Mater.*, **20**, 4135 (2008)
101. S.P.Albu, H.Tsuchiya, S.Fujimoto, P.Schmuki. *Eur. J. Inorg. Chem.*, 4351 (2010)
102. D.I. Petukhov, A.A.Eliseev, I.V.Kolesnik, K.S.Napolskii, A.V.Lukashin, Y.D.Tretyakov, S.V.Grigoriev, N.A.Grigorieva, H.Eckerlebe. *Microporous Mesoporous Mater.*, **114**, 440 (2008)
103. I.V.Kolesnik. Candidate Theses in Chemical Sciences, MSU, Moscow, 2010
104. M.Zhang, G.Yao, Y.Cheng, Y.Xu, L.Yang, J.Lv, S.Shi, X.Jiang, G.He, P.Wang, X.Song, Z.Sun. *Appl. Surface. Sci.*, **356**, 546 (2015)
105. L.Li, J.Ya, F.Hu, Z.Liu, E.Lei. *J. Energy Chem.*, **25**, 740 (2016)
106. C.-C.Chen, W.C.Say, S.-J.Hsieh, E.W.-G.Diau. *Appl. Phys. A Mater. Sci. Process.*, **95**, 889 (2009)
107. W.C.Say, C.-C.Chen, Y.H.Shiu. *Jpn. J. Appl. Phys.*, **48**, 035004 (2009)
108. M.Stancheva, M.Bojinov. *J. Solid State Electrochem.*, **17**, 1271 (2013)
109. P.Acevedo-Peña, L.Lartundo-Rojas, I.González *J. Solid State Electrochem.*, **17**, 2939 (2013)
110. V.C.Anitha, A.N.Banerjee, G.R.Dillip, S.W.Joo, B.K.Min. *J. Phys. Chem. C*, **120**, 9569 (2016)
111. A.Ghicov, S.P.Albu, R.Hahn, D.Kim, T.Stergiopoulos, J.Kunze, C.-A.Schiller, P.Falaras, P.Schmuki. *Chem. – Asian J.*, **4**, 520 (2009)
112. C.M.Teh, A.R.Mohamed. *J. Alloys Compd.*, **509**, 1648 (2011)
113. Y.Yalcin, M.Kilic, Z.Cina. *Appl. Catal., B*, **99**, 469 (2010)
114. C.Fan, P.Xue, Y.Sun. *J. Rare Earths*, **24**, 309 (2006)
115. Z.M.El-Bahy, A.A.Ismail, R.M.Mohamed. *J. Hazard. Mater.*, **166**, 138 (2009)
116. J.G.Yu, Q.J.Xiang, M.H.Zhou, *Appl. Catal., B*, **90**, 595 (2009)
117. J.-N.Nian, S.-A.Chen, C.-C.Tsai, H.Teng. *J. Phys. Chem. B*, **110**, 25817 (2006)
118. S.N.R.Inturi, T.Boningari, M.Suidan, P.G.Smirniotis. *Appl. Catal., B*, **144**, 333 (2014)
119. Y.F.Su, Z.Wu, Y.N.Wu, J.D.Yu, L.Sun, C.J.Lin. *J. Mater. Chem. A*, **3**, 8537 (2015)
120. K.E.Karakitsou, X.E.Verykios. *J. Phys. Chem.*, **97**, 1184 (1993)
121. Y.Furubayashi, T.Hitosugi, Y.Yamamoto, K.Inaba, G.Kinoda, Y.Hirose, T.Shimada, T.Hasegawa. *Appl. Phys. Lett.*, **86**, 252101 (2005)
122. A.R.Bally, E.N.Korobeinikova, P.E.Schmid, F.Levy, F.Bussy. *J. Phys. D: Appl. Phys.*, **31**, 1149 (1998)
123. N.S.Kozhevnikova, E.A.Kozlova, A.A.Valeeva, A.A.Lemke, A.S.Vorokh, S.V.Cherepanova, T.P.Lyubina, E.V.Gerasimov, S.V.Tsybulya, A.A.Remplel. *Dokl. Chem.*, **440**, 278 (2011)
124. F.Wang, D.G.Li. *Mater. Lett.*, **158**, 119 (2015)
125. S.W.Shin, J.Y.Lee, K.S.Ahn, S.H.Kang, J.H.Kim. *J. Phys. Chem. C*, **119**, 13375 (2015)
126. R.Ramanathan, V.Bansal. *RSC Adv.*, **5**, 1424 (2015)
127. B.Gao, X.X.Li, Y.W.Ma, Y.Cao, Z.Y.Hu, X.M.Zhang, J.J.Fu, K.F.Huo, P.K.Chu. *Thin Solid Films*, **584**, 61 (2015)
128. J.Hu, H.S.Li, Q.Wu, Y.Zhao, Q.Z.Jiao. *Chem. Eng. J.*, **263**, 144 (2015)
129. R.Asahi, T.Morikawa, T.Ohwaki, K.Aoki, Y.Taga. *Science*, **293**, 269 (2001)
130. M.Shen, Z.Wu, H.Huang, Y.Du, Z.Zou, P.Yang. *Mater. Lett.*, **60**, 693 (2006)
131. R.Asahi, T.Morikawa. *Chem. Phys.*, **339**, 57 (2007)
132. J.C.Yu, J.Yu, W.Ho, Z.Jiang, L.Zhang. *Chem. Mater.*, **14**, 3808 (2002)
133. A.Ghicov, S.Aldabergenova, H.Tsuchiya, P.Schmuki. *Angew. Chem.*, **118**, 7150 (2006)
134. A.Ghicov, S.Aldabergenova, H.Tsuchyia, P.Schmuki. *Angew. Chem., Int. Ed.*, **45**, 6993 (2006)
135. K.Yasuda, P.Schmuki. *Adv. Mater.*, **19**, 1757 (2007)
136. T.Caronna, C.Gambarotti, L.Palmisano, C.Punta, M.Pierini, F.Recupero. *J. Photochem. Photobiol. A*, **189**, 322 (2007)
137. H.Yin, Y.Wada, T.Kitamura, S.Kambe, S.Murasawa, H.Mori, T.Sakata, S.Yanagida. *J. Mater. Chem.*, **11**, 1694 (2001)
138. S.Yurdakal, G.Palmisano, V.Loddo, O.Alagöz, V.Augugliaro, L.Palmisano. *Green Chem.*, **11**, 510 (2009)
139. J.M.Macak, M.Zlamal, J.Krysa, P.Schmuki. *Small*, **3**, 300 (2007)
140. H-ch.Liang, X.-zh.Li. *J. Hazard. Mater.*, **162**, 1415 (2009)
141. S.Sreekantan, R.Hazan, Z.Lockman. *Thin Solid Films*, **518**, 16 (2009)
142. S.Sarker, B.Mukherjee, E.Crone, V.Subramanian. *J. Mater. Chem. A*, **2**, 4890 (2014)
143. Y.Yang, W.Y.Wang. *J. Power Sources*, **293**, 577 (2015)
144. P.Pathak, S.Gupta, K.Grosulak, H.Imahori, V.Subramanian. *J. Phys. Chem. C*, **119**, 7543 (2015)
145. Z.B.Shao, W.Zhu, Z.Li, Q.H.Yang, G.Z.Wang. *J. Phys. Chem. C*, **116**, 2438 (2012)
146. D.H.Kim, H.S.Han, I.S.Cho, W.M.Seong, I.J.Park, J.H.Park, S.Shin, G.D.Park, S.Park, S.Lee, K.S.Hong. *Int. J. Hydrogen Energy*, **40**, 863 (2015)
147. Y.Xie, G.Ali, S.H.Yoo, S.O.Cho. *ACS Appl. Mater. Interfaces*, **2**, 2910 (2010)
148. Y.Liu, L.Zhao, M.T.Li, L.J.Guo. *Nanoscale*, **6**, 7397 (2014)
149. H.-S.Rao, W.-Q.Wu, Y.Liu, Y.-F.Xu, B.-X.Chen, H.-Y.Chen, D.-B.Kuang, C.-Y.Su. *Nano Energy*, **8**, 1 (2014)
150. K.Miller, K.S.Nalwa, A.Bergerud, N.M.Neihart, S.Chaudhary. *IEEE Electron Device Lett.*, **31**, 737 (2010)
151. V.Aglieri, A.Zaffora, G.Lullo, M.Santamaria, F.Di Franco, U.L.Cicero, M.Mosca, R.Macaluso. *Superlatt. Microstruct.*, **113**, 135 (2018)
152. Y.Yu, F.Yang, S.Mao, S.Zhu, Y.Jia, L.Yuan, M.Salmen, B.Sun. *Chem. Phys. Lett.*, **706**, 477 (2018)
153. D.Chu, A.Younis, S.Li. *J. Phys. D: Appl. Phys.*, **45** (35), 355306 (2012)
154. J.E.Yoo, K.Lee, A.Tighineanu, P.Schmuki. *Electrochem. Commun.*, **34**, 177 (2013)
155. N.Liu, K.Lee, P.Schmuki. *Angew. Chem., Int. Ed.*, **52**, 12381 (2013)
156. A.S.Vokhmintsev, I.A.Weinstein, R.V.Kamalov, I.B.Dorosheva. *Bull. Russ. Acad. Sci.: Phys.*, **78**, 932 (2014)
157. D.Conti, A.Lamberti, S.Porro, P.Rivolo, A.Chiolerio, C.F.Pirri, C.Ricciardi. *Nanotechnology*, **27**, 485208 (2016)
158. I.B.Dorosheva, A.S.Vokhmintsev, R.V.Kamalov, A.O.Gryaznov, I.A.Weinstein. In *Proceedings — 2018 Ural Symposium on Biomedical Engineering, Radioelectronics and Information Technology, USBEREIT 2018*. (Yekaterinburg, 2018). P. 279
159. J.Chen, Y.Wu, K.Zhu, F.Sun, C.Guo, X.Wu, G.Cheng, R.Zheng. *Electrochim. Acta*, **316**, 133 (2019)
160. A.Hazra, A.Jan, A.Tripathi, S.Kundu, P.K.R.Boppidi, S.Gangopadhyay. *IEEE Trans. Electron Devices*, **67**, 2197 (2020)
161. K.M.Kim, G.H.Kim, S.J.Song, J.Y.Seok, M.H.Lee, J.H.Yoon, C.S.Hwang. *Nanotechnology*, **21**, 305203 (2010)
162. K.M.Kim, B.J.Choi, M.H.Lee, G.H.Kim, S.J.Song, J.Y.Seok, J.H.Yoon, S.Han, C.S.Hwang. *Nanotechnology*, **22**, 254010 (2011)
163. X.-B.Yin, K.Tian, Z.-H.Tan, R.Yang, X.Guo. *J. Electrochem. Soc.*, **162**, E271 (2015)
164. V.K.Sahu, A.K.Das, R.S.Ajimsha, P. Misra. *J. Phys. D: Appl. Phys.*, **51**, 215101 (2018)

165. V.A.Milichko, A.S.Shalin, I.S.Mukhin, A.E.Kovrov, A.A.Krasilin, A.V.Vinogradov, P.A.Belov, C.R.Simovski. *Phys. Usp.*, **59**, 727 (2016)
166. S.A.Gavrilov, A.A.Dronov, V.I.Shevyakov, A.N.Belov, E.A.Poltoratskii. *Nanotechnol. Russ.*, **4** (3 – 4), 237 (2009)
167. Y.Liu, Y.Cheng, W.Shu, Z.Peng, K.Chen, J.Zhou, W.Chen, G.S. Zakharova. *Nanoscale*, **6**, 6755 (2014)
168. T.Nikolay, L.Larina, O.Shevaleevskiy, B.T.Ahn. *Energy Environ. Sci.*, **4**, 1480 (2011)
169. X.Liu, J.Fang, Y.Liu, T.Lin. *Front. Mater. Sci.*, **10**, 225 (2016)
170. V.R.Subramanian, S.Sarker, B.Yu, A.Kar, X.Sun, S.K.Dey. *J. Mater. Res.*, **28**, 280 (2013)
171. J.Lin, X.Liu, S.Zhu, X.Chen. *Nanotechnol. Rev.*, **4**, 209 (2015)
172. L.Zheng, S.Han, H.Liu, P.Yu, X.Fang. *Small*, **12**, 1527 (2016)
173. C.Xu, P.H.Shin, L.Cao, J.Wu, D.Gao. *Chem. Mater.*, **22**, 143 (2010)
174. J.R.Jennings, A.Ghicov, L.M.Peter, P.Schmuki, A.B.Walker. *J. Am. Chem. Soc.*, **130**, 13364 (2008)
175. D.Kuang, J.Brillet, P.Chen, M.Takata, S.Uchida, H.Miura, K.Sumioka, S.M.Zakeeruddin, M.Grätzel. *ACS Nano*, **2**, 1113 (2008)
176. X.Gao, J.Li, J.Baker, Y.Hou, D.Guan, J.Chen, C.Yuan. *Chem. Commun.*, **50**, 6368 (2014)
177. Y.Hwang, Y.H.Park, H.S.Kim, D.H.Kim, S.Ali, S.Sorcar, M.C.Flores, M.R.Hoffmann, S.-I.In. *Chem. Commun.*, **56**, 7080 (2020)
178. F.Giordano, A.Abate, J.P.Correa Baena, M.Saliba, T.Matsui, S.H.Im, S.M.Zakeeruddin, M.K.Nazeeruddin, A.Hagfeldt, M.Graetzel. *Nat. Commun.*, **7**, 10379 (2016)
179. I.Turkevych, S.Kazaoui, N.A.Belich, A.Y.Grishko, S.A.Fateev, A.A.Petrov, T.Urano, S.Aramaki, S.Kosar, M.Kondo, E.A.Goodilin, M.Graetzel, A.B.Tarasov. *Nat. Nanotechnol.*, **14**, 57 (2019)
180. Q.Zhang, R.Chen, H.San, G.Liu, K.Wang. *J. Power Sources*, **282**, 529 (2015)
181. Y.Ma, N.Wang, J.Chen, C.Chen, H.San, J.Chen, Z.Cheng. *ACS Appl. Mater. Interfaces*, **10**, 22174 (2018)
182. N.Wang, Y.Ma, J.Chen, C.Chen, H.San, J.Chen, Z.Cheng. *Nanoscale*, **10**, 13028 (2018)
183. C.Chen, N.Wang, H.San, Z.Cheng. In *2016 IEEE SENSORS*. (Orlando, 2016). No. 7808427
184. C.Chen, N.Wang, P.Zhou, H.San, K.Wang, X.Chen. *ACS Appl. Mater. Interfaces*, **8**, 24638 (2016)
185. A.Krasnov, S.Legotin, K.Kuzmina, N.Ershova, B.Rogozev. *Nucl. Eng. Technol.*, **51**, 1978 (2019)
186. M.V.S.Chandrashekhar, C.I.Thomas, Li.Hui, M.G.Spencer, A.Lal. *Appl. Phys. Lett.*, **88**, 033506 (2006)
187. Z.Cheng, X.Chen, H.San, Z.Feng, B.Liu. *J. Micromech. Microeng.*, **22**, 074011 (2012)
188. V.Bormashov, S.Troschiev, A.Volkov, S.Tarelkin, E.Korostylev, A.Golovanov, M.Kuznetsov, D.Teteruk, N.Kornilov, S.Terentiev, S.Buga, V.Blank. *Phys. Status Solidi, A*, **212**, 2539 (2015)
189. A.A.Krasnov, S.A.Legotin. *Instrum. Exp. Technol.*, **63** (4), 437 (2020)
190. C.Clement Raj, R.Prasanth. *J. Electrochem. Soc.*, **165**, E345 (2018)
191. H.Wu, D.Li, X.Zhu, C.Yang, D.Liu, X.Chen, Y.Song, L.Lu. *Electrochim. Acta*, **116**, 129 (2014)
192. H.Zhou, Y.Zhang. *J. Phys. Chem. C*, **118**, 5626 (2014)
193. M.Salari, K.Konstantinov, H.K.Liu. *J. Mater. Chem.*, **21**, 5128 (2011)
194. X.Lu, G.Wang, T.Zhai, M.Yu, J.Gan, Y.Tong, Y.Li. *Nano Lett.*, **12**, 1690 (2012)
195. A.Tamilselvan, S.Balakumar. *Ionics*, **22**, 99 (2016)
196. M.Salari, S.H.Aboutalebi, K.Konstantinov, H.K.Liu. *Phys. Chem. Chem. Phys.*, **13**, 5038 (2011)
197. C.Zhang, L.Li, C.-C.Tuan, J.Zhou, F.Xue, C.-P.Wong. *J. Mater. Sci. Mater. Electron.*, **29**, 15130 (2018)
198. W.Li, W.Zhang, T.Li, A.Wei, Y.Liu, H.Wang. *Nanoscale Res. Lett.*, **14**, 229 (2019)
199. N.T.Nguyen, S.Ozkan, I.Hwang, X.Zhou, P.Schmuki. *Mater. Chem. A*, **5**, 1895 (2017)
200. H.Fan, S.Zhang, X.Zhu. *Chem. Phys. Lett.*, **730**, 340 (2019)
201. Y.Xie, Y.Wang, H.Du. *Mater. Sci. Eng. B: Solid State Mater. Adv. Technol.*, **178**, 1443 (2013)
202. F.Tian, Y.Xie, H.Du, Y.Zhou, C.Xia, W.Wang. *RSC Adv.*, **4**, 41856 (2014)
203. W.Zhong, S.Sang, Y.Liu, Q.Wu, K.Liu, H.Liu. *J. Power Sources*, **294**, 216 (2015)
204. X.Ning, X.Wang, X.Yu, J.Li, J.Zhao. *J. Alloys Compd.*, **658**, 177 (2016)
205. C.Zhang, S.Tian, C.Xu, L.Li, J.Zhou, F.Xue. *J. Mater. Sci.-Mater. Electron.*, **30**, 20892 (2019)
206. Z.Li, Y.Ding, W.Kang, C.Li, D.Lin, X.Wang, Z.Chen, M.Wu, D.Pan. *Electrochim. Acta*, **161**, 40 (2015)
207. S.P.Hong, S.Kim, N.Kim, J.Yoon, C.Kim. *Korean J. Chem. Eng.*, **36**, 1753 (2019)
208. H.Wu, C.Xu, J.Xu, L.Lu, Z.Fan, X.Chen, Y.Song, D.Li. *Nanotechnology*, **24**, 455401 (2013)
209. J.Xu, H.Wu, L.Lu, S.-F.Leung, D.Chen, X.Chen, Z.Fan, G.Shen, D.Li. *Adv. Funct. Mater.*, **24**, 1840 (2014)
210. H.Zhou, X.Zou, Y.Zhang. *Electrochim. Acta*, **192**, 259 (2016)
211. J.Zhang, Y.Wang, Y.Qin, C.Yu, L.Cui, X.Shu, J.Cui, H.Zheng, Y.Zhang, Y.Wu. *J. Solid State Chem.*, **246**, 269 (2017)
212. Z.-D.Gao, X.Zhu, Y.-H.Li, X.Zhou, Y.-Y.Song, P.Schmuki. *Chem. Commun.*, **51**, 7614 (2015)
213. K.Trzciński, M.Szkoda, A.P.Nowak, M.Łapiński, A.Lisowska-Oleksiak. *Beilstein J. Nanotechnol.*, **10**, 483 (2019)
214. Z.Zhang, Z.Xu, Z.Yao, Y.Meng, Q.Xia, D.Li, Z.Jiang. *J. Alloys Compd.*, **805**, 396 (2019)
215. Z.Gao, Z.Cui, S.Zhu, Y.Liang, Z.Li, X.Yang. *J. Power Sources*, **283**, 397 (2015)
216. H.Tang, M.Xiong, D.Qu, D.Liu, Z.Zhang, Z.Xie, X.Wei, W.Tu, D.Qu. *Nano Energy*, **15**, 75 (2015)
217. G.Wang, H.Feng, L.Hu, W.Jin, Q.Hao, A.Gao, X.Peng, W.Li, K.-Y.Wong, H.Wang, Z.Li, P.K.Chu. *Nat. Commun.*, **9**, 2055 (2018)
218. F.Gobal, M.Faraji. *Ionics*, **21**, 525 (2015)
219. Y.Xie, H.Du. *J. Solid State Electrochem.*, **16**, 2683 (2012)
220. R.B.Ambade, S.B.Ambade, N.K.Shrestha, Y.-C.Nah, S.-H.Han, W.Lee, S.-H.Lee. *Chem. Commun.*, **49**, 2308 (2013)
221. R.B.Ambade, S.B.Ambade, N.K.Shrestha, R.R.Salunkhe, W.Lee, S.S.Bagde, J.H.Kim, F.J.Stadler, Y.Yamauchi, S.-H.Lee. *Mater. Chem. A*, **5**, 172 (2017)
222. Y.Gao, K.Ding, X.Xu, Y.Wang, D.Yu. *RSC Adv.*, **4**, 27130 (2014)
223. Z.Shao, H.Li, M.Li, C.Li, C.Qu, B.Yang. *Energy*, **87**, 578 (2015)
224. K.Gulati, Y.Zhang, P.Di, Y.Liu, S.Ivanovski. *ACS Biomater. Sci. Eng.*, (2021); https://doi.org/10.1021/acsbiomaterials.1c00529
225. D.Chopra, K.Gulati, S.Ivanovski. *Acta Biomater.*, **127**, 80 (2021)
226. A.Jayasree, S.Ivanovski, K.Gulati. *J. Control. Release*, **333**, 521 (2021)
227. J.Park, A.Cimpean, A.B.Tesler, A.Mazare. *Nanomaterials*, **11**, 2359 (2021)
228. E.A.Nunes Simonetti, T.Cardoso de Oliveira, Á.Enrico do Carmo Machado, A.A.Coutinho Silva, A.Silva dos Santos, L.de Simone Cividanes. *Ceram. Int.*, **47**, 17844 (2021)
229. P.V.Govardhana Reddy, B.Rajendra Prasad Reddy, M.Venkata Krishna Reddy, K.Raghava Reddy, N.P.Shetti, T.A.Saleh, T.M.Aminabhavi. *J. Environ. Manag.*, **279**, 111603 (2021)
230. S.Palmas, L.Mais, M.Mascia, A.Vacca. *Curr. Opin. Electrochem.*, **28**, 100699 (2021)

231. N.T.Sahrin, R.Nawaz, F.K.Chong, S.L.Lee, M.D.H.Wirzal. *Environ. Technol. Innov.*, **22**, 101418 (2021)
232. K.Siuzdak, Ł.Haryński, J.Wawrzyniak, K.Grochowska. *Prog. Solid State Chem.*, **62**, (2021)
233. J. Prakash, S.Samriti, A.Kumar, H.Dai, B.C.Janegitz, V.Krishnan, H.C.Swart, S.Sun. *Mater. Today Sust.*, **13**, 100066 (2021)
234. X.Nie, S.Yin, W.Duan, Z.Zhao, L.Li, Zh.Zhang. *Nano*, **16** (1), 2130002 (2021); https://doi.org/10.1142/S1793292021300024
235. Y.Xu, G.Zangari. *Coatings*, **11**, 931 (2021)
236. A.Lavacchi, M.Bellini, E.Berretti, Y.Chen, A.Marchionni, H.A.Miller, F.Vizza. *Curr. Opin. Electrochem.*, **28**, 100720 (2021)
237. M.M.Zhang, J.Y.Chen, H.Li, C.R.Wang. *Rare Metals*, **40**, 249 (2021)
238. P.Bamola, B.Singh, A.Bhoumik, M.Sharma, C.Dwivedi, M.Singh, G.K.Dalapati, H.Sharma. *ACS Appl. Nano Mater.*, **3**, 10591 (2020)